

IMPROVING THE FUNCTION FOR GRAIN BOUNDARY ENERGY  
INTERPOLATION IN URANIUM DIOXIDE

by

Jarin French

A senior thesis submitted to the faculty of

Brigham Young University - Idaho

in partial fulfillment of the requirements for the degree of

Bachelor of Science

Department of Physics

Brigham Young University - Idaho

December 2016



Copyright © 2016 Jarin French

All Rights Reserved



BRIGHAM YOUNG UNIVERSITY - IDAHO

DEPARTMENT APPROVAL

of a senior thesis submitted by

Jarin French

This thesis has been reviewed by the research committee, senior thesis coordinator, and department chair and has been found to be satisfactory.

---

Date

---

Evan Hansen, Advisor

---

Date

---

David Oliphant, Senior Thesis Coordinator

---

Date

---

Matt Zachreson, Committee Member

---

Date

---

Stephen McNeil, Chair



## ABSTRACT

# IMPROVING THE FUNCTION FOR GRAIN BOUNDARY ENERGY INTERPOLATION IN URANIUM DIOXIDE

Jarin French

Department of Physics

Bachelor of Science

Efforts have been made to find an interpolary function for the grain boundary (GB) energies of uranium dioxide, based on work done by Bulatov *et al.*[Acta Mater. 65, 161 (2014)]. A MATLAB<sup>®</sup> script developed by Harbison[B.S. Thesis, Brigham Young University - Idaho (2015)] and Bulatov *et al.* was used to perform this work. Molecular dynamics data was collected using the LAMMPS (Large-scale Atomic/Molecular Massively Parallel Simulation) program developed at Sandia National Laboratory. Results for the  $\langle 100 \rangle$ ,  $\langle 110 \rangle$ , and  $\langle 111 \rangle$  symmetric tilt and twist GBs have been collected. The new data sets were calculated with an 800 K anneal which allowed the atoms to relax to a lower energy state. An improved fit is found for the  $\langle 100 \rangle$  and  $\langle 110 \rangle$  symmetric tilt sets and the  $\langle 110 \rangle$  twist set, whereas the  $\langle 100 \rangle$  twist and  $\langle 111 \rangle$  symmetric tilt and twist sets show unexpected trends. Further research needs to be done for the  $\langle 100 \rangle$  and  $\langle 111 \rangle$  sets to determine why the fitting procedure does not accurately reflect the expected results. Additional research should also be done to determine if outlying data points necessitate fitting additional cusps.





## ACKNOWLEDGMENTS

I would first like to thank the Department of Energy Office of Science for the Visiting Faculty Program (VFP) - Student, and the Nuclear Energy Advanced Modeling and Simulation (NEAMS) programs which allowed me this research opportunity. Thanks also goes to Brigham Young University - Idaho and Idaho National Laboratory for providing me with the necessary facilities to do this work. I would especially like to thank my mentor Dr. Yongfeng Zhang for his patience and guidance as I have worked on this research. Additionally I would like to thank Dr. Evan Hansen, John-Michael Bradley, and Dr. Xianming Bai for their valuable contributions to my understanding. Finally, I would like to thank my wife who has been so supportive of me as I have spent so much time doing this work, and who has been a constant source of strength to me.



# Contents

<b>Table of Contents</b>	<b>xi</b>
<b>List of Figures</b>	<b>xiii</b>
<b>1 Introduction</b>	<b>1</b>
1.1 Background . . . . .	3
1.2 Previous Work . . . . .	6
<b>2 Methods</b>	<b>7</b>
2.1 Molecular Dynamics . . . . .	7
2.2 Bulatov <i>et al.</i> 's Methods . . . . .	9
2.3 Representations of Grain Boundary Space . . . . .	10
2.3.1 Axis-Angle Representation . . . . .	11
2.3.2 Rodrigues Representation . . . . .	12
2.3.3 Fundamental Zone Representation . . . . .	13
2.4 Code Analysis . . . . .	13
2.4.1 The Fitting Code . . . . .	13
2.4.2 The Energy Calculation Code . . . . .	14
2.5 Reduced Chi-Square Statistic . . . . .	15
2.5.1 Developing the P and Q Matrices . . . . .	15
2.5.2 Calculating Reduced Chi Squared . . . . .	20
<b>3 Results and Discussion</b>	<b>23</b>
3.1 Validation of P and Q Matrices . . . . .	23
3.2 Fitting Results . . . . .	23
3.3 Reduced Chi-square Results . . . . .	26
<b>4 Conclusion</b>	<b>29</b>
<b>Bibliography</b>	<b>31</b>
<b>A List of Parameters</b>	<b>35</b>
<b>B Graphs</b>	<b>39</b>
<b>C Orientation Matrix Generator</b>	<b>45</b>

D genOrientationMatrix.sh Bash Script
---------------------------------------

65
----

# List of Figures

1.1	An image representing the fluorite crystal structure. For $\text{UO}_2$ , the smaller spheres indicate the uranium atoms, and the larger spheres indicate the oxygen atoms. Image courtesy of the University of Cambridge under the Creative Commons license. . . . .	3
1.2	A representation of GBs, where (a) shows an example of a grain boundary and (b) shows an example of GB types. In (a) individual atoms of the grains are the circles, while the grain boundary is highlighted by the line. Atomic mismatch between the differently oriented grains causes an excess of energy to be present within the material, which has an effect on the material's properties. Image courtesy of the University of Cambridge under the Creative Commons license. In (b) the axis of rotation for the tilt GB (top) is perpendicular to the GB normal, and for the twist GB (bottom) is parallel to the GB normal. Image courtesy of Wikipedia under the Creative Commons license. . . . .	5
2.1	These figures demonstrate example crystal structures of $\text{UO}_2$ after an annealing process. The better the atoms line up, the lower the energy is. (a) shows an example of a mostly aligned GB, indicative of a lower energy. (b) shows an example of a misaligned GB, indicative of a higher energy. These two images are from a $\langle 111 \rangle$ twist image. Different viewpoints show different amounts of alignment. The LAMMPS simulation package takes care of all the calculations to determine the energy at these GBs. Images courtesy of Dr. Evan Hansen, used with permission. . . . .	8
2.2	Figure 2 from Bulatov <i>et al.</i> <sup>1</sup> (a) demonstrates the theoretical relationship between the high-symmetry subsets of the 5D GB space. Each multi-dimensional subset is interpolated from smaller-dimensional subsets. (b) shows the Rodrigues space representation of the fundamental zone of all GBs as built from three high-symmetry axes ( $\langle 100 \rangle$ , $\langle 110 \rangle$ , and $\langle 111 \rangle$ ). The unit vectors along the axis identify the boundary plane inclination in the frame of grain one. A parallel vector thus represents a twist boundary, a perpendicular vector represents a tilt boundary, and neither parallel nor perpendicular vectors represent a mixed boundary. The full misorientation space has 1152 symmetrically equivalent copies of the fundamental zone <sup>1,2</sup> which allows the infinite nature of Rodrigues space to be accounted for. . . . .	10

2.3	An example of an RSW function with $\theta_{min} = 0^\circ$ , $\theta_{max} = 15^\circ$ , and $a$ (the shaping parameter) = 0.5 Combining these functions into a Piecewise set over a given domain gives the GB energy curves their distinct, cusp-like behavior. The RSW functions are scaled using $E_{min}$ and $E_{max}$ . In this example, $E_{min} = 0$ and $E_{max} = 1$ . . . . .	11
2.4	A geometric method of determining the normals of a GB. (a) to (c) show the GB normals for a GB perpendicular to the axis of rotation (a twist GB). The GB normal is simply the axis about which the grains are rotated. (d) and (e) show the GB normals for a GB parallel to the axis of rotation (a tilt GB). The GB normal is perpendicular to the axis of rotation. The same GB normal for $\langle 110 \rangle$ Tilt can be used for $\langle 111 \rangle$ Tilt. . . . .	18
3.1	The $\langle 100 \rangle$ twist (a) and tilt (b) results for the P and Q matrices as compared to Bulatov <i>et al.</i> 's energy profiles. The expected value was calculated using Bulatov <i>et al.</i> 's GB5DOF.m MATLAB <sup>®</sup> script with the default values. The calculated values were found by inputting the matrices into the GB5DOF.m script. With the exception of the data points at $1^\circ$ in both (a) and (b) and $89^\circ$ in (b), the energies calculated from the matrices matches the expected curves exactly. . . . .	24
3.2	The $\langle 100 \rangle$ twist (a) and tilt (b) results. In general the re-calculated energies are lower, with significant differences around $40^\circ$ to $50^\circ$ in the tilt subset. The positive concavity in the twist subset around $40^\circ$ is unexpected, and may indicate the presence of a missing cusp. There is a possible cusp around $30^\circ$ in the twist subset, and around $68^\circ$ in the tilt subset. . . . .	26
3.3	A comparison of the expected value of the fitted function with the values calculated using the P and Q matrices for the $\langle 100 \rangle$ 1D tilt subset. The MD values are shown for reference. There is a scaling issue yet to be fixed, but it is uncertain what is causing the scaling issue for this subset. . . . .	26
3.4	An comparison of current fitting functions with a possible change to the functions. Original functions are shown as the dashed lines, with the updated functions shown as the solid lines. MD results are shown for reference. (a) shows a possible change from the Read-Shockley-Wolf (RSW) functions to a simple square root function multiplied by an exponential decay. There is no theoretical basis behind this change however. (b) attempts to fit to a cusp around $40^\circ$ . Further work can be done to find a better fit for this subset. (c) shows the most potential improvement. The potential fit increases the total number of parameters by three to fit to the cusp around $28^\circ$ . A quick glance at the MD values compared to the fit shows a great improvement from the current fit. . . . .	27

B.1	The $\langle 100 \rangle$ twist (a) and tilt (b) results for the P and Q matrices as compared to Bulatov <i>et al.</i> 's energy profiles. The expected value was calculated using Bulatov <i>et al.</i> 's GB5DOF.m MATLAB <sup>®</sup> script with the default values. The calculated values were found by inputting the matrices into the GB5DOF.m script. With the exception of the data points at $1^\circ$ in both (a) and (b) and $89^\circ$ in (b), the energies calculated from the matrices matches the expected curves exactly. . . . .	39
B.2	The $\langle 110 \rangle$ twist (a) and tilt (b) results for the P and Q matrices as compared to Bulatov <i>et al.</i> 's energy profiles. The expected value was calculated using Bulatov <i>et al.</i> 's GB5DOF.m MATLAB <sup>®</sup> script with the default values. The calculated values were found by inputting the matrices into the GB5DOF.m script. With the exception of the data points at $1^\circ$ in both (a) and (b) and $179^\circ$ in (b), the energies calculated from the matrices matches the expected curves exactly. . . . .	40
B.3	The $\langle 111 \rangle$ twist (a) and tilt (b) results for the P and Q matrices as compared to Bulatov <i>et al.</i> 's energy profiles. The expected value was calculated using Bulatov <i>et al.</i> 's GB5DOF.m MATLAB <sup>®</sup> script with the default values. The calculated values were found by inputting the matrices into the GB5DOF.m script. With the exception of the data points at $1^\circ$ in both (a) and (b) and $60^\circ$ in (b), the energies calculated from the matrices matches the expected curves exactly. . . . .	40
B.4	The $\langle 100 \rangle$ twist (a) and tilt (b) results. In general the re-calculated energies are lower, with significant differences around $40^\circ$ to $50^\circ$ in the tilt subset. The positive concavity in the twist subset around $40^\circ$ is unexpected, and may indicate the presence of a missing cusp. There is a possible cusp around $30^\circ$ in the twist subset, and around $68^\circ$ in the tilt subset. . . . .	41
B.5	The $\langle 110 \rangle$ twist (a) and tilt (b) results. Significant decreases in energy are found for both subsets. Possible cusp locations are around $40^\circ$ in the twist subset, and around $40^\circ$ , $90^\circ$ , and $140^\circ$ in the tilt subset. . . . .	41
B.6	The $\langle 111 \rangle$ twist (a) and tilt (b) results. Some energies are found to be lower, but some are also found to be higher. The positive concavity present in these results is unexpected, and could indicate the presence of cusps. A possible location for the twist subset is around $33^\circ$ . Additional data is needed to determine possible cusp locations for the tilt subset. . . . .	42
B.7	A comparison of the expected value of the fitted function with the values calculated using the P and Q matrices for the $\langle 100 \rangle$ 1D subsets. The MD values are shown for reference. (a) PQ results follow exactly the fitted curve. (b) has a scaling issue yet to be fixed. It is uncertain what is causing the scaling issue for this subset. . . . .	42

- 
- B.8 A comparison of the expected value of the fitted function with the values calculated using the P and Q matrices for the  $\langle 110 \rangle$  1D subsets. MD values are shown for reference. (a) follows the fitted result until the cusp, at which point some anomalies appear. The results from the PQ matrices dip well below the expected value at the cusp, and never make it back to the original fitted line. (b) has a similar issue on a lesser scale. Only two of the calculated points do not follow the fitted curve. The endpoint is expected to return a zero value, where the PQ matrices calculated a value slightly higher. There is also an unexpected cusp from the PQ matrices in the middle of the second hump. All other data points follow the fitted curve exactly. . . . . 43
- B.9 A comparison of the expected value of the fitted function with the values calculated using the P and Q matrices for the  $\langle 111 \rangle$  1D subsets. MD values are shown for reference. (a) closely follows the expected fitted values, but has a slight error throughout. (b) follows the expected values exactly in the center of the fitting, but misses slightly for lower angle boundaries, and misses completely at the end. . . . . 44



# Chapter 1

## Introduction

Nuclear energy has long been of interest to the world as a possible source of energy. Despite the promise of a long-term solution to the renewable-energy problem, fears still grip the hearts of civilians and government officials across the world because of the nuclear bombs used on Japan during World War II, and because of nuclear reactor catastrophes such as Three Mile Island, Chernobyl, and most recently Fukushima. A major part of addressing these fears focuses on making the operation of nuclear reactors more safe. Part of the concern with nuclear energy is the radioactivity associated with nuclear materials, so minimal exposure to the material is sought after. “Minimal exposure” in part means efficient use of nuclear fuel, spreading out the time between refueling, and limiting radiation exposure to human and machine alike. Extensive studies (past and present) of nuclear fuels seek to achieve the safety and efficiency sought after with this major energy source.

In order for a nuclear reactor to work properly, many things need to be taken into consideration. First, understanding the ideal operating conditions for the nuclear reactor is important so immediate actions can be taken when conditions are no longer ideal. Radioactivity has an effect on all materials, not just living tissue. Over time, radiation can create defects in the crystal structures of the metals used to create the reactor shell, and these defects can build up, causing deformation, weakening, or stiffening of the materials, which

can lead to problems if not properly managed.<sup>3</sup> As the reactions continue, more neutrons are created, potentially causing additional fission events. In order to prevent the reactor from having all the fuel fission at nearly the same time (releasing a large amount of energy), various methods control the number of chain reactions. Emergency procedures also prevent catastrophes as mentioned above.

Second, the quality of the fuel must meet a minimum standard in order for a sustainable reaction to occur. Nuclear fuels come in one of two categories: fissile (where bombardment of the material with neutrons will divide the atomic nuclei into “daughter” particles, releasing energy), and non-fissile (bombardment of the material results in the neutrons becoming part of the nucleus, called absorption). Nuclear reactors require fissile materials to work. One of the most common fissile materials is an isotope of uranium called U-235. A second isotope of uranium, U-238, is much more common (approximately 99% of all uranium). In order to have a sustainable chain-reaction, the amount of U-235 present in fuel must be at a certain level, depending on the moderating medium.<sup>4</sup>

Third, the various properties of the fuel need to be well understood in order to make the running of the reactor as safe and effective as possible. Some of these properties include thermal conductivity (how well heat flows through the material), fission gas release (how some of the fission products move throughout the material as gases), and mechanical stability (i.e. how the material bends or cracks under pressure or heat). Taking thermal conductivity as an example, knowledge of this material property allows the most effective use of coolant to keep the reactor within operating temperatures, maximizing both efficiency and safety. Knowledge of other material properties allows for similar gains in efficiency, safety, or both.

Uranium dioxide ( $\text{UO}_2$ ) is the primary choice for nuclear fuel in today’s reactors.<sup>4</sup> In order to understand the properties of  $\text{UO}_2$  as described above, an analysis of the basic crystal structure of the material is required.  $\text{UO}_2$  is a ceramic, meaning that a series of crystal lattices join together in various ways to create the material. This material has a fluorite crystal structure, where the uranium atoms form a face-centered cubic (fcc) lattice,

and the oxygen atoms form a simple cubic lattice within the fcc frame (see Figure 1.1). This work adds to the safety and efficiency of using nuclear energy by providing the necessary information to accurately calculate the material properties of  $\text{UO}_2$  in-reactor.



**Figure 1.1** An image representing the fluorite crystal structure. For  $\text{UO}_2$ , the smaller spheres indicate the uranium atoms, and the larger spheres indicate the oxygen atoms. Image courtesy of the University of Cambridge under the Creative Commons license.

## 1.1 Background

Ceramics, metals, and polymers are composed of tiny crystals called *grains*. The orientation of each grain is generally independent of the orientation in the grains surrounding it, creating a possibility (depending on how the crystal formed<sup>3</sup>) that crystal structures will not line up at the interfaces where these two grains meet. This “atomic mismatch”<sup>3</sup> leads to broken or stretched atomic bonds where atoms will not line up relative to a perfect crystal structure. These defects are called grain boundaries (GBs), and an illustration of a GB is shown in Figure 1.2a. The most popular way to parameterize a GB uses the five degree-of-freedom (DoF) model.<sup>1,5–9</sup> This model only uses the macroscopic DoFs (the observable DoFs corresponding

to the misorientation and inclination), ignoring the three translational DoFs (the ability of the grain to move or slide anywhere in space) possessed by each grain. Three of the five DoFs specify the misorientation (or misalignment) of the grains with respect to each other. The other two DoFs specify the orientation of the grain boundary plane (called the inclination). The misorientation DoFs consist of the rotation angle  $\theta$  (one of three) and the rotation axis (another two angles, where the first angle is measured in the  $xy$ -plane perpendicular to the  $z$  axis, and the second angle is measured from the positive  $z$ -axis), while the normal of the GB defines the inclination DoFs (two angles).<sup>6</sup>

Three specific types of GBs occur in polycrystalline materials: twist, tilt, and mixed GBs.<sup>6,9</sup> These GBs describe the misorientation of two grains with respect to each other. Twist boundaries have the axis of rotation between the two grains and the GB normal parallel to each other. Tilt boundaries can be either symmetric and asymmetric. A tilt boundary occurs when the axis of rotation between the two grains is perpendicular to the GB normal. Symmetric tilt boundaries describe a GB whose boundary plane is a mirror plane: one side of the boundary mirrors the other. This makes the angles between the boundary plane and the orientation axes of the two grains equal. Asymmetric tilt boundaries have unequal angles. Figure 1.2b shows a representation of tilt boundaries (top) and twist boundaries (bottom). A mixed GB is a combination of twist and tilt boundaries in some degree.

Understanding GBs is important because of the effects they have on material properties.<sup>1,5,7</sup> The crystal structure has extra energy because of the atomic mismatch at the boundaries. This extra energy, called GB energy, gives rise to GB motion. Knowing and predicting how the GBs will move allows for more accurate calculations of a material's properties. Thus, GB energy needs to be understood in order to accurately model the evolution of material properties.

Two methods of modeling GB energy are the isotropic and anisotropic models. The most common method (and easier method) is the isotropic model. This model ignores the impact of inclination on the GB energy, and assumes equal inclinations for a given misorientation,

reducing the five-dimensional (5D) parameter space to a three-dimensional (3D) parameter space. The reasons for assuming this model historically was based on the assumption that the inclination had little or no impact on the GB energy, or (later) that it was too difficult to create a full five DoF model.<sup>7</sup> Alternatively, the anisotropic approach seeks to quantify the effect that misorientation *and* inclination have on the GB energy. Currently researchers acknowledge the need for a full five DoF model for the GB energy, but assert the difficulty inherent in developing such a model.<sup>6,7,9</sup> Despite these difficulties, GB energy functions for certain materials, namely fcc metals copper, gold, aluminum, and nickel, have proven successful.<sup>1</sup>

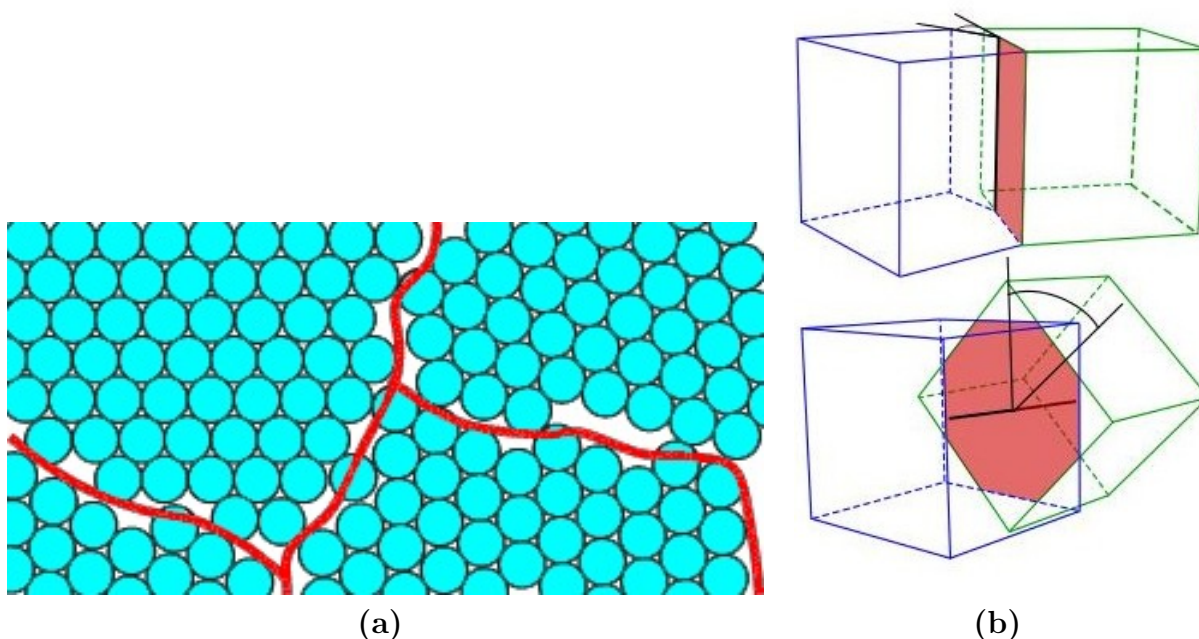


**Figure 1.2** A representation of GBs, where (a) shows an example of a grain boundary and (b) shows an example of GB types. In (a) individual atoms of the grains are the circles, while the grain boundary is highlighted by the line. Atomic mismatch between the differently oriented grains causes an excess of energy to be present within the material, which has an effect on the material's properties. Image courtesy of the University of Cambridge under the Creative Commons license. In (b) the axis of rotation for the tilt GB (top) is perpendicular to the GB normal, and for the twist GB (bottom) is parallel to the GB normal. Image courtesy of Wikipedia under the Creative Commons license.

## 1.2 Previous Work

Bulatov *et al.*<sup>1</sup> developed a five DoF function which accurately interpolates GB energies for certain fcc metals. They used energies for GBs along specific axes to interpolate the full 5D GB space. Chapter 2 explains their methods in more detail. Harbison<sup>8</sup> applied Bulatov *et al.*'s methods to calculate similar parameters to describe the full five DoF GB space for  $\text{UO}_2$ . GB energies for various misorientations around a high-symmetry axis were gathered using molecular dynamics (MD) simulations. The fitting procedure created a set of 43 parameters defining the function needed to interpolate an arbitrary GB energy.

This work improves the fitting parameters by using MD results calculated by Zhang<sup>10</sup> and Hansen<sup>11</sup> with an anneal of 800K. Harbison's data did not anneal the crystal structure,<sup>8</sup> which prevented the atoms from finding their ideal energetic minimum. The 800 K anneal allows the atoms to relax to a value closer to their global minimum, as shown in Chapter 3. A database will store these simulated energies, and a MATLAB<sup>®</sup> script will use the database to fit the function parameters. Idaho National Laboratory (INL) will incorporate the updated parameters into its mesoscale phase field modeling platform MARMOT for use in modeling nuclear fuels. As these parameters are implemented in the modeling software, various tests of the  $\text{UO}_2$  fuel can determine how the material properties change while in-reactor.

# Chapter 2

## Methods

Sufficient data is a requirement for any fitting procedure, but unfortunately there is a lack of data on uranium dioxide ( $\text{UO}_2$ ) grain boundary (GB) energies in the literature. Molecular dynamics (MD) simulations<sup>10,11</sup> were used as fitting data to calculate the GB energies of various lattices based on the coincident site lattice (CSL) model. This model is built off of the idea that GB energy is low when more lattice sites are in coincidence. A number defined as the  $\Sigma$ -number describes the number of coincident sites per total number of lattice sites in a given unit cell of a crystal.<sup>6,9</sup> A MATLAB<sup>®</sup> script, developed using Bulatov *et al.*'s methods<sup>1</sup> and building off of Harbison's<sup>8</sup> script, used the gathered data.

### 2.1 Molecular Dynamics

Simulation results from the Large-scale Atomic/Molecular Massively Parallel Simulation (LAMMPS) software (developed at Sandia National Laboratory<sup>12</sup>) were gathered for a number of twist, tilt, and mixed GBs. These calculations were performed by creating two crystals of  $\text{UO}_2$  and placing them together in various orientations. A GB is introduced at the interface, creating GB energy. The energy of the system is calculated from the interatomic forces inside the crystal. That energy is compared to the energy of a single grain (of the same size as the combined two grains) of  $\text{UO}_2$  in order to determine the energy at the GB.<sup>8</sup>

The difference between these two values divided by twice the area of the GB gives the GB energy of the particular misorientation.<sup>13</sup> An example of how the atoms align is shown in Figure 2.1. Harbison's original calculations<sup>8</sup> were done using no anneal (maximum temperature was approximately 0K), only allowing the atoms to relax to their local minima. This work used an anneal of 800K, allowing the atoms to relax to a better estimate of their global minimum value as is shown in Figures B.4 to B.6. The misorientation angles at which these energies were calculated were the same as used in the work of Harbison. These energies are used in the fitting procedure to produce parameters describing the five-dimensional GB space.

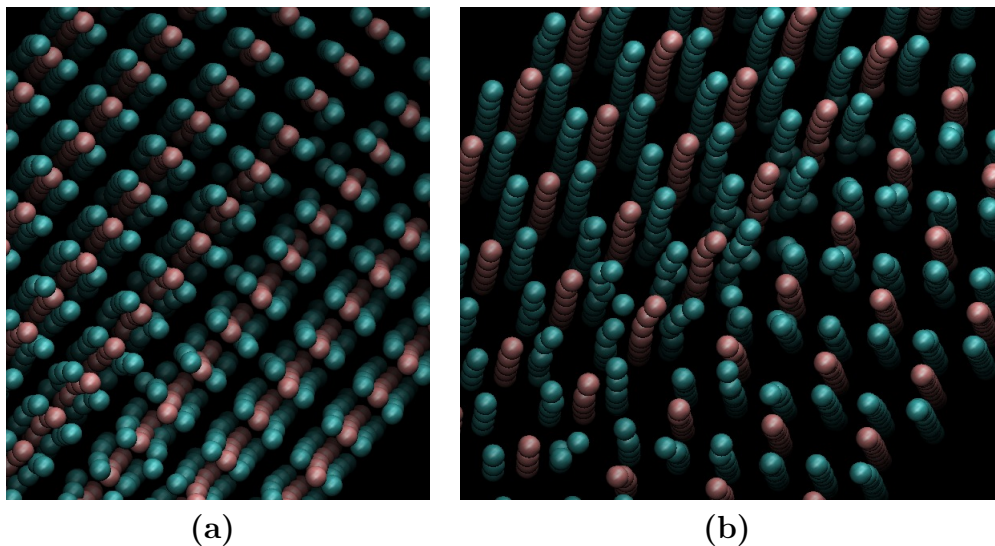


**Figure 2.1** These figures demonstrate example crystal structures of  $\text{UO}_2$  after an annealing process. The better the atoms line up, the lower the energy is. (a) shows an example of a mostly aligned GB, indicative of a lower energy. (b) shows an example of a misaligned GB, indicative of a higher energy. These two images are from a  $\langle 111 \rangle$  twist image. Different viewpoints show different amounts of alignment. The LAMMPS simulation package takes care of all the calculations to determine the energy at these GBs. Images courtesy of Dr. Evan Hansen, used with permission.



## 2.2 Bulatov *et al.*'s Methods

In order to find the energy of an arbitrary GB in the five-space, Bulatov *et al.*<sup>1</sup> implemented a hierarchical interpolation method. They started by choosing three three-dimensional (3D) high-symmetry axes to use as scaffolding to build the entire five-dimensional (5D) function. The axes chosen were the  $\langle 100 \rangle$ ,  $\langle 110 \rangle$ , and the  $\langle 111 \rangle$  sets for their four-, two-, and three-fold rotational symmetries respectively.\* Each 3D subset is built from an interpolation of their own one- and two-dimensional subsets. The symmetric tilt and twist GBs for each set were fitted first because of their simplicity. Only the rotation angle is needed to fully define the energies for these subsets, making them one-dimensional (in Figure 2.2a, the darker bands in the smaller circles). From the symmetric tilt subset, the asymmetric, or general, tilt subset was interpolated. A second rotation angle defining the rotation of the second grain makes this subset two-dimensional (the lighter, wider band of color around the symmetric subset). A combination of the general tilt subset (two dimensions) and the twist subset (one dimension) was used to interpolate the 3D subset for each high-symmetry axis (the three smaller circles). These three 3D subsets were then used to interpolate the GB 5D space.

Read and Shockley<sup>15</sup> initially developed the equations used to do the interpolation (called Read-Shockley functions) to describe the GB energy at low-angle boundaries (The definition of a “low-angle boundary” varies from material to material. Boundaries with angles higher than<sup>9</sup> 6° up to<sup>16</sup> 15° have been cited as low-angle boundaries). Wolf developed a method<sup>16</sup> using Read-Shockley functions to calculate the energies at high-angle boundaries, with the resulting functions being called Read-Shockley-Wolf (RSW) functions. These RSW functions take the form:

$$E_{min} + (E_{max} - E_{min}) \sin \left( \frac{\pi}{2} \frac{\theta - \theta_{min}}{\theta_{max} - \theta_{min}} \right) \left( 1 - a \log \left( \sin \left( \frac{\pi}{2} \frac{\theta - \theta_{min}}{\theta_{max} - \theta_{min}} \right) \right) \right), \quad (2.1)$$

---

\*For cubic crystals, rotations of 90°, 180°, or 120° about any  $\langle 100 \rangle$ ,  $\langle 110 \rangle$ , or  $\langle 111 \rangle$  axis respectively is a symmetry operation.<sup>14</sup> Thus, the  $\langle 100 \rangle$  set is four-fold symmetric ( $360^\circ/90^\circ=4$ ), the  $\langle 110 \rangle$  set is two-fold symmetric ( $360^\circ/180^\circ=2$ ), and the  $\langle 111 \rangle$  set is three-fold symmetric ( $360^\circ/120^\circ=3$ ).

where  $\theta$  is the misorientation angle,  $\theta_{min}$  is the minimum angle on the domain,  $\theta_{max}$  is the maximum angle on the domain, and  $a$  is a shaping parameter. Each of Wolf's RSW functions cover a “low-angle” subset of the domain of the 1D GB space. An example of a simple RSW function is shown in Figure 2.3. Multiple RSW functions are stitched together to form the 1D subsets.

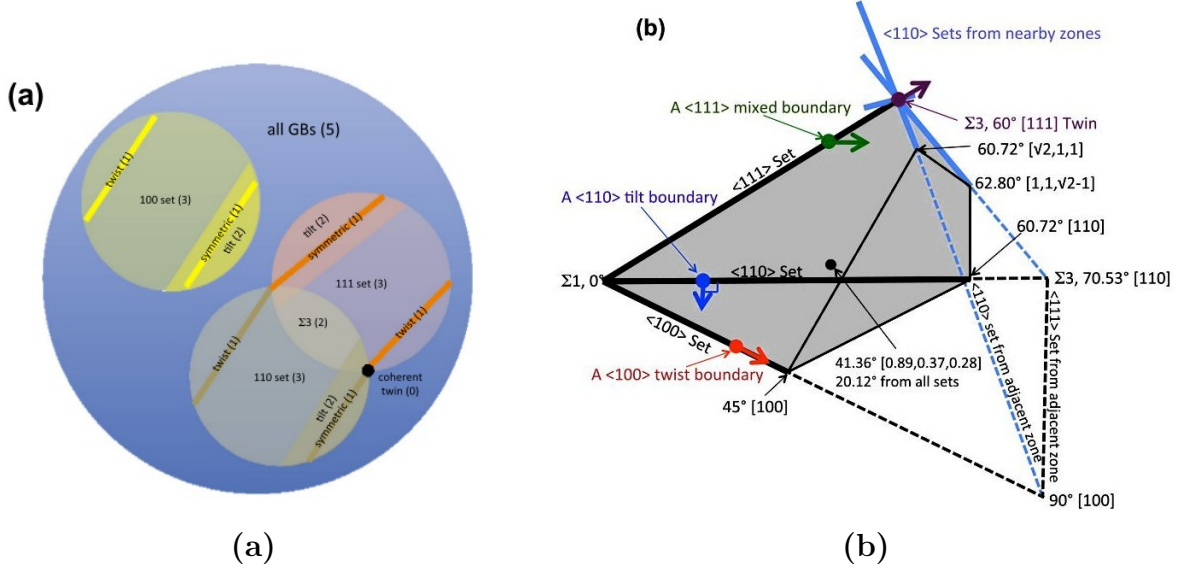


**Figure 2.2** Figure 2 from Bulatov *et al.*<sup>1</sup> (a) demonstrates the theoretical relationship between the high-symmetry subsets of the 5D GB space. Each multi-dimensional subset is interpolated from smaller-dimensional subsets. (b) shows the Rodrigues space representation of the fundamental zone of all GBs as built from three high-symmetry axes ( $\langle 100 \rangle$ ,  $\langle 110 \rangle$ , and  $\langle 111 \rangle$ ). The unit vectors along the axis identify the boundary plane inclination in the frame of grain one. A parallel vector thus represents a twist boundary, a perpendicular vector represents a tilt boundary, and neither parallel nor perpendicular vectors represent a mixed boundary. The full misorientation space has 1152 symmetrically equivalent copies of the fundamental zone<sup>1,2</sup> which allows the infinite nature of Rodrigues space to be accounted for.

## 2.3 Representations of Grain Boundary Space

Part of the development of this 5D function was accomplished through visual representations of the GB space. However, the size of the five-space in which GBs reside makes representing them difficult. Different methods have been developed to represent them, each with their

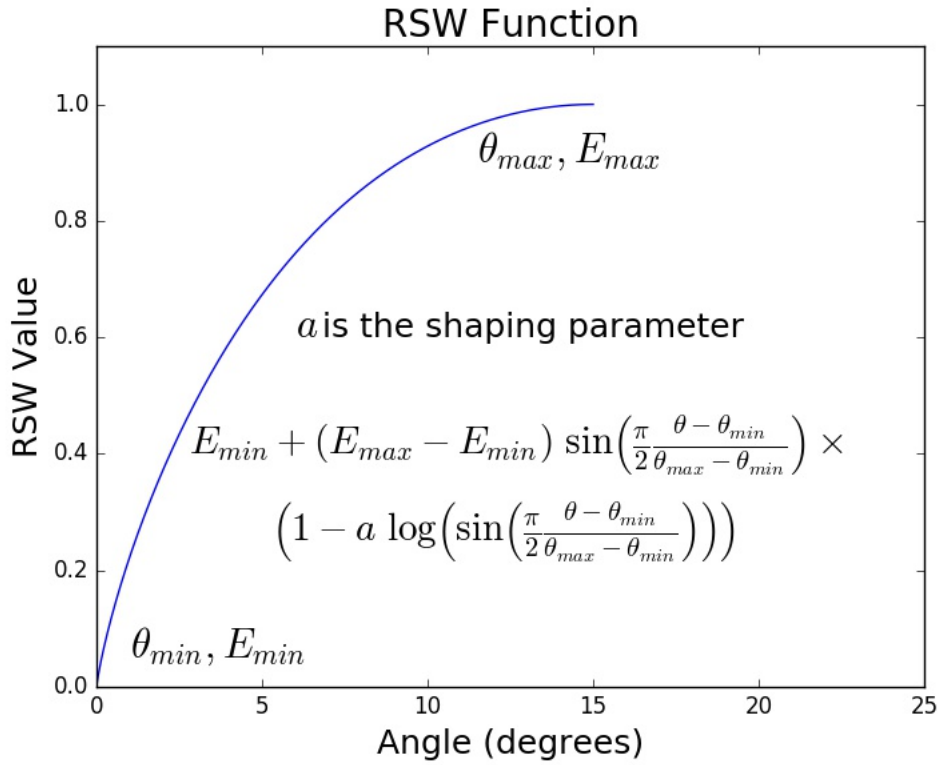


**Figure 2.3** An example of an RSW function with  $\theta_{min} = 0^\circ$ ,  $\theta_{max} = 15^\circ$ , and  $a$  (the shaping parameter) = 0.5 Combining these functions into a Piecewise set over a given domain gives the GB energy curves their distinct, cusp-like behavior. The RSW functions are scaled using  $E_{min}$  and  $E_{max}$ . In this example,  $E_{min} = 0$  and  $E_{max} = 1$ .

advantages and disadvantages. Three of these methods are the axis-angle representation, the Rodrigues representation, and the fundamental zone representation. These methods, though described separately, can be used together to form a better picture of what the GB space looks like (see for example Figure 2.2b which combines the Rodrigues representation and the fundamental zone representation).

### 2.3.1 Axis-Angle Representation

The axis-angle representation is the simplest of the three described here. The axis of rotation of the GB specifies the point in axis-angle space, and the angle of misorientation between the two grains at the GB specifies the magnitude of the vector. Thus, the axis ( $\mathbf{a}$ , where

$\mathbf{a}$  has components  $a_x$ ,  $a_y$ , and  $a_z$ ) and the angle ( $\theta$ ) mathematically represent an axis-angle vector as:

$$\mathbf{A} = \mathbf{a} \theta \quad (2.2)$$

The axis-angle space can only take into account three degrees of freedom: the two angles specifying the axis, and the angle rotated through. Thus, axis-angle space cannot fully visualize all of the necessary information contained in the full 5D space.<sup>17</sup> An added difficulty of using this representation is its infinite space because it is a mapping of an axis and an angle onto a Cartesian coordinate system. This mapping means understanding the entire GB space is nearly impossible without the help of additional methods. The axis-angle representation is best used as a starting point to move to other, more robust representations, and to represent the misorientation between two grains.<sup>2</sup>

### 2.3.2 Rodrigues Representation

The Rodrigues representation (sometimes called the “Rodrigues-Frank” representation) uses Rodrigues vectors to represent rotations in Rodrigues space. This representation takes ideas from the axis-angle space, but makes a few changes allowing crystal symmetries to be taken into account. The axis about which a GB is oriented still specifies the point in space, but the tangent of half the angle represents the magnitude of the vector. Thus, a Rodrigues vector can be represented as:<sup>2,17-20</sup>

$$\mathbf{R} = \mathbf{a} \tan \left( \frac{\theta}{2} \right) \quad (2.3)$$

Some researchers favor this representation over others because of the lack of curvature such a mapping entails.<sup>2,17</sup> However, still only three of the five degrees of freedom are specified. A unit vector at the points along the axis represents the other two in Figure 2.2b. A parallel vector represents a twist boundary, and a perpendicular vector represents a tilt boundary. Anything else represents a mix of twist and tilt (or a mixed boundary). One difficulty in using Rodrigues space is it also is an infinite space, as it simply maps an axis and an angle onto a Cartesian coordinate system.<sup>17,21</sup>

### 2.3.3 Fundamental Zone Representation

The fundamental zone is perhaps the best graphical representation for the 5D GB. This representation takes advantage of the symmetries inherent in crystals<sup>14</sup> to simplify an infinite space into a compact, finite area called the fundamental zone.<sup>1,5,7,18,22</sup> Every point within the space represents a unique orientation, and every point outside the space can be represented as a point inside the space through symmetry operations.<sup>17-19</sup> Bulatov *et al.* used this idea in connection with Rodrigues space to create Figure 2.2b. In Rodrigues space, the crystal symmetric of the material determine the shape of the fundamental zone.<sup>5,18</sup> For fcc crystals, the fundamental zone takes the form of a truncated tetrahedron.<sup>1</sup> The edges of the fundamental zone in Rodrigues space represent the high-symmetry rotation axes, and points on one face can represent another point on a different face of the fundamental zone.

## 2.4 Code Analysis

Harbison's<sup>8</sup> and Bulatov *et al.*'s<sup>1</sup> MATLAB<sup>®</sup> scripts were used in this work. These codes were analyzed to understand the process for both fitting the GB energy parameters, and for calculating the GB energy of an arbitrary GB.

### 2.4.1 The Fitting Code

An extensive analysis of Harbison's<sup>8</sup> code was conducted to learn how it worked. The basic outline for how the fit occurs is as follows. First, data is read in from a database containing energies associated with either a twist or tilt GB on one of the three high-symmetry axes. Test parameters which are used as starting points are also read in from a separate database. The one-dimensional sets are fitted first because of their simplicity. The parameters found from the 1D fits are used in fitting the higher-dimensional sets. Important angles are specified where low energies are expected, such as the  $\Sigma 5$  boundary for the  $\langle 100 \rangle$  symmetric tilt subset. These angles are calculated based on the  $\Sigma$ -number from CSL theory. Because

the  $\Sigma$ -number designates how many lattice points are between each coincident site (and assuming that the space between each lattice site, the lattice constant, is known) the angle of the GB misorientation can be determined. In order to minimize the potential for error in calculations, every energy in the parameter-vector is listed as a scaled value based on the  $e_{RGB}$  parameter – a parameter representing the energy of an arbitrary, random GB, and can be seen as an average of the GB energies. Thus, to make relevant comparisons, the energies are unscaled based on the units of energy desired (typically J/m<sup>2</sup>). An initial step size is then set, and data for the specific subsets is read in from a database. All of the parameters and the angle-energy pairs are then passed into a grid-search fitting function. Each subset had a different initial step size to avoid a numerical error where the steps would take the angles currently being looked at outside of their domain.

Once the six one-dimensional subsets and the three two-dimensional subsets are fitted, the three-dimensional subsets are fitted using the twist and asymmetric tilt subsets to calculate the mixing parameters (defining the relationship between the twist and general tilt subsets within a high-symmetry axis - i.e. the relationship between the small dark bands representing the twist boundaries and the lighter, wider bands representing the tilt boundaries in Figure 2.2a). The final step is to calculate the weighting parameters, which defines the relationship between the three high-symmetry subsets. Equations defining the various relationships can be found in Bulatov *et al.*'s work.

### 2.4.2 The Energy Calculation Code

Bulatov *et al.*'s open-source MATLAB<sup>®</sup> code<sup>1</sup> calculates the energy of an arbitrary GB in an fcc metal. The same procedure is used for calculating an arbitrary GB in uranium dioxide, and goes as follows. First, metrics defining the “distance” between the GB and all three high-symmetry axes are calculated. These distances are calculated by looking at all symmetrically equivalent representations of a GB on a per-axis basis (for cubic crystals, there are 24 equivalent representations<sup>14</sup>). Because there are three, six, and four unique axes

for the  $\langle 100 \rangle$ ,  $\langle 110 \rangle$ , and  $\langle 111 \rangle$  axes respectively, a maximum of  $6 \times 24 = 144$  distances are calculated. Those distances exceeding a predefined cutoff distance are discarded. After all distances have been calculated, only the unique representations are kept to avoid double-counting certain representations.<sup>1</sup> Energies are calculated for each unique distance in each subset. These energies are then weighted and summed together to give the interpolated energy for the specified GB.

## 2.5 Reduced Chi-Square Statistic

A good way to test how well a function fits the data is to use a reduced chi-square goodness-of-fit statistic.<sup>23</sup> In order to calculate this statistic the orientation matrices (which Bulatov *et al.* calls the P and Q matrices for the first and second grain respectively) were needed as input parameters to Bulatov *et al.*'s function. These three by three matrices specify the orientation in a lab frame of the two grains individually. A good fit will have a reduced chi-square value close to one, while those values greater than one indicate an under fit, and those values less than one indicate an over fit.<sup>23</sup>

### 2.5.1 Developing the P and Q Matrices

Creating the P and Q matrices was a non-trivial task. Because there has been so much work done with crystallography over the past few decades, many different methods have been developed to specify the orientation matrices of grains. A rotation matrix also needed to be calculated which rotates the axis of rotation to the  $[100]$  direction, as Bulatov *et al.*'s energy calculation code assumes. Three methods, following the method prescribed in MARMOT, using the Rodrigues rotation formula, and using the Bunge rotation matrix were used in the process of developing these matrices are described below.

## MARMOT Method

MARMOT, Idaho National Laboratory's (INL's) mesoscale phase-field modeling platform,<sup>24</sup> calculates the P and Q matrices for the grains using Euler angles as input parameters. The Euler angles are converted to the orientation matrices using the Bunge convention, i.e. the  $ZXZ$  or  $ZX'Z''$  rotation, where the first rotation is about the  $z$  axis, the second rotation is around the new  $x$  axis, and the final rotation is about the new  $z$  axis. The formula for this conversion from Bunge Euler angles to the rotation matrix is found by multiplying the  $z$ ,  $x$ , and  $z$  rotation matrices together in that order to get:

$$\begin{bmatrix} c_1 c_3 - c_2 s_1 s_3 & -c_1 s_3 - c_2 c_3 s_1 & s_1 s_2 \\ c_3 s_1 + c_1 c_2 s_3 & c_1 c_2 c_3 - s_1 s_3 & -c_1 s_2 \\ s_2 s_3 & c_3 s_2 & c_2 \end{bmatrix} \quad (2.4)$$

where  $c_n$  and  $s_n$  represent the cosine and sine of the respective angles (1 represents the first  $z$  rotation, 2 represents the  $x$  rotation, and 3 represents the second  $z$  rotation. These angles are usually referred to as<sup>2</sup>  $\varphi_1, \Phi, \varphi_2$ ).

The rotation matrix was calculated in MARMOT by using the GB normal and finding the rotation matrix required to rotate that vector to the  $[100]$  direction. In MARMOT, simulations are set up through input files. In the input files there are different sections (called blocks) specifying material parameters, boundary conditions, initial conditions, and what physics to use to solve the problem (among others). The initial condition used to calculate the rotation matrices in MARMOT was a horizontal or vertical line for tilt or twist boundaries respectively. Because of this set up, the GB normals were either along the  $[010]$  axis for the tilt boundaries, or  $[\bar{1}00]$  for twist boundaries.



### Rodrigues Rotation Formula

The Rodrigues rotation formula<sup>25</sup> (RRF) is a way of calculating the rotation matrices given an axis and an angle using the following formula:

$$\mathbf{R} = \mathbf{I} + \sin \theta \mathbf{K} + (1 - \cos \theta) \mathbf{K}^2, \quad (2.5)$$

where  $\mathbf{I}$  is the 3x3 identity matrix,  $\theta$  is the angle rotated through, and  $\mathbf{K}$  is the skew-symmetric matrix formed by the axis of rotation ( $\mathbf{a}$ ) by:

$$\begin{bmatrix} 0 & -a_z & a_y \\ a_z & 0 & -a_x \\ -a_y & a_x & 0 \end{bmatrix} \quad (2.6)$$

The rotation matrices were calculated two different ways with this orientation matrix formulation. One method was to simply use the MARMOT-generated rotation matrices. These rotation matrices Another method was to calculate the rotation matrices using geometric arguments (see Figure 2.4). From these arguments the normals are identified in Table 2.1.

### Bunge Rotation Matrix

The Bunge rotation matrix (see Equation (2.4)) is what MARMOT uses to create the orientation matrices. There were various methods used to calculate the Euler angles, of which three are briefly described here. The Euler angles (once calculated) were used in the first two methods to calculate the entirety of the rotation matrix.

The first method tried was to use scripts developed to calculate the various Euler angles for MARMOT. These scripts did not work because of the same assumptions made earlier about the orientation of the GB, namely, that all pure tilt GBs have a normal of 010, and that all pure twist GBs have a normal of  $\bar{1}00$ . The difference between MARMOT's boundary conditions and the boundary conditions of this work is that GBs in this work are assumed to be either perpendicular or parallel to the rotation axis, as opposed to always being along the x or y axis.

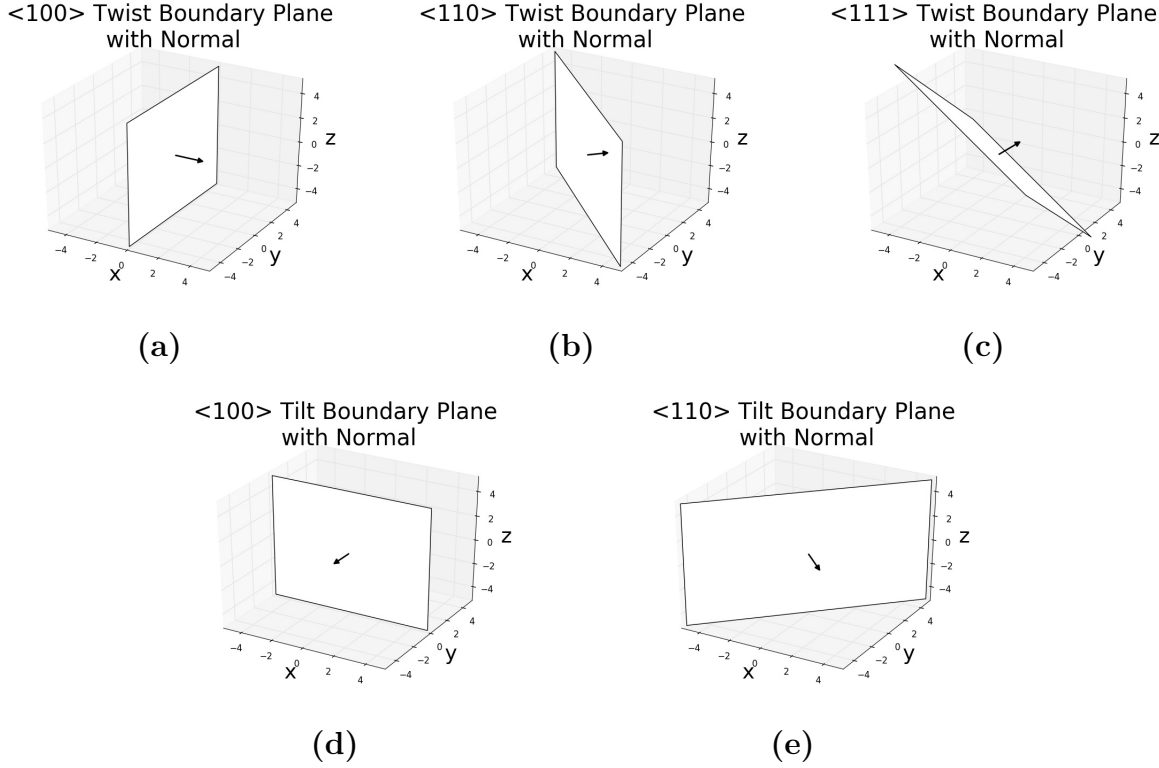


**Figure 2.4** A geometric method of determining the normals of a GB. (a) to (c) show the GB normals for a GB perpendicular to the axis of rotation (a twist GB). The GB normal is simply the axis about which the grains are rotated. (d) and (e) show the GB normals for a GB parallel to the axis of rotation (a tilt GB). The GB normal is perpendicular to the axis of rotation. The same GB normal for  $\langle 110 \rangle$  Tilt can be used for  $\langle 111 \rangle$  Tilt.

The second method was to use an open-source MATLAB<sup>®</sup> package called MTEX.<sup>26</sup> This package calculates Euler angles using quaternions. These Euler angles did not generate the correct results either, for the most part creating the same sorts of graphs as the MARMOT method. It is uncertain why this method did not work.

The working method used the mathematics of quaternions.<sup>27</sup> The quaternions were calculated directly based on the misorientation axis and angle. A quaternion is a four-dimensional vector containing one real part, and three imaginary parts. The components of the vector are calculated as follows:

$$\mathbf{q} = \left[ \cos \left( \frac{\theta}{2} \right), a_x \sin \left( \frac{\theta}{2} \right), a_y \sin \left( \frac{\theta}{2} \right), a_z \sin \left( \frac{\theta}{2} \right) \right], \quad (2.7)$$

with axis  $\mathbf{a}$  and misorientation angle  $\theta$ . Once the axis and misorientation angle are con-

**Table 2.1** Table of GB normals for different GB types. The normalized dot product of the axis with the GB normal is zero in all tilt cases and one in all twist cases. There are two options for the grain boundary normals of each subset because of inversion symmetries.

Axis	Boundary Type	GB Normal
$\langle 100 \rangle$	Tilt	$[010]$
		$[0\bar{1}0]$
$\langle 110 \rangle$	Tilt	$[1\bar{1}0]$
		$[\bar{1}10]$
$\langle 111 \rangle$	Tilt	$[1\bar{1}0]$
		$[\bar{1}10]$
$\langle 100 \rangle$	Twist	$[100]$
		$[\bar{1}00]$
$\langle 110 \rangle$	Twist	$[110]$
		$[\bar{1}\bar{1}0]$
$\langle 111 \rangle$	Twist	$[111]$
		$[\bar{1}\bar{1}\bar{1}]$

verted to a quaternion, another conversion from a quaternion to the Bunge Euler angles is performed. The angles are calculated using the `atan2` method which allows for all four quadrants in the Cartesian space to be accounted for. The angles are calculated using the following formulas:

$$\begin{aligned}
 \chi &= \sqrt{(q_0^2 + q_3^2)(q_1^2 + q_2^2)} \\
 \varphi_1 &= \text{atan2} \left( \frac{q_0 q_2 + q_1 q_3}{2\chi}, \frac{q_0 q_1 - q_2 q_3}{2\chi} \right) \\
 \Phi &= \text{atan2} (2\chi, q_0^2 + q_3^2 - q_1^2 - q_2^2) \\
 \varphi_2 &= \text{atan2} \left( \frac{q_1 q_3 - q_0 q_2}{2\chi}, \frac{q_0 q_1 + q_2 q_3}{2\chi} \right).
 \end{aligned} \tag{2.8}$$

Once the Euler angles were calculated, they were put into Equation (2.4), and the result-

ing matrices were used as the orientation for the grains. The codes used to generate the orientation matrices can be found in Appendices C and D.

### Testing The Matrices

In order to test the different methods, an attempt was made to reproduce the 1D subset graphs as shown in Bulatov *et al.*. Various levels of success were observed for the different methods. The matrices giving the best results are shown in Figure 3.1 and ????.

While the first method works well for MARMOT, the challenge accompanying its use was that MARMOT specifies a specific GB normal with the set up of the problem that is not necessarily what the MATLAB® script expects. Thus, the results coming from using this combination of matrices ended up working only for the  $\langle 100 \rangle$  tilt,  $\langle 110 \rangle$  tilt, and  $\langle 100 \rangle$  twist subsets, while the  $\langle 110 \rangle$  twist had issues with singularities, and the  $\langle 111 \rangle$  subsets did not remotely match the expected outcome.

### 2.5.2 Calculating Reduced Chi Squared

There were two methods used to calculate the  $\chi_{red}^2$  statistic. The first method was to use the P and Q matrices as developed above to test the entirety of the fit. The second method was to calculate the statistic for each 1D subset, then calculate the full  $\chi_{red}^2$  value using the statistics from the subsets. Results from these calculations are discussed in the next chapter.

The test for the entire fit was done using the P and Q matrices to calculate the energy in  $1^\circ$  intervals for each subset, using the GB5D0F.m script. The difference between the calculated values and the MD values was calculated, and the  $\chi_{red}^2$  value was calculated for each subset and for the entire fit, producing the results in Table 3.1 under the 800 K anneal column under the “ $\chi_{red}^2$  using P and Q matrices” section.

Using the second method, the same angles used in the fitting procedure were used in the RSW equations creating the 1D subsets. The differences between the values resulting from there and the MD simulation values lead to the  $\chi_{red}^2$  values shown in the 800 K anneal

column under the  $\chi^2_{\text{red}}$  comparing the 1D fits section. The same methods were implemented to calculate the  $\chi^2_{\text{red}}$  values for the data without an anneal.

The statistic calculated using these methods is different from the  $\chi^2$  statistic used in the grid-search function. The grid search used Equation (2.9), and generated values of the same order as Equation (3.1).

$$\chi^2 = \sum (E_{\text{measured}} - E_{\text{calculated}})^2 \quad (2.9)$$



# Chapter 3

## Results and Discussion

### 3.1 Validation of P and Q Matrices

The energy profiles calculated from the P and Q matrices were compared with the copper energy profiles expected from the parameters defined in Bulatov *et al.*'s code to validate the generated P and Q matrices. Results from this comparison for the  $\langle 100 \rangle$  set are shown in Figure 3.1, with all six subsets shown in Figures B.1 to B.3. The calculated energies match exactly the predicted values for all but a few points. Each data set mismatches the expected energy at  $1^\circ$ , and the tilt data sets also see this mismatch at their second to last data point.

### 3.2 Fitting Results

Comparisons for the one-dimensional (1D) results from Harbison<sup>8</sup> and this work are presented in Figure 3.2 for the  $\langle 100 \rangle$  subset. Appendix B has the full set of comparison graphs shown in Figures B.4 to B.6. The results show a general decrease in the grain boundary (GB) energies, allowing trends in the different subsets to emerge. These trends allow for an all around better fit, but there are still some unexpected results present. The parameters calculated from the fitting procedure are shown in Table A.1 in Appendix A.

Initial MD recalculations of the  $\langle 100 \rangle$  symmetric tilt GB energies using the 800 K anneal

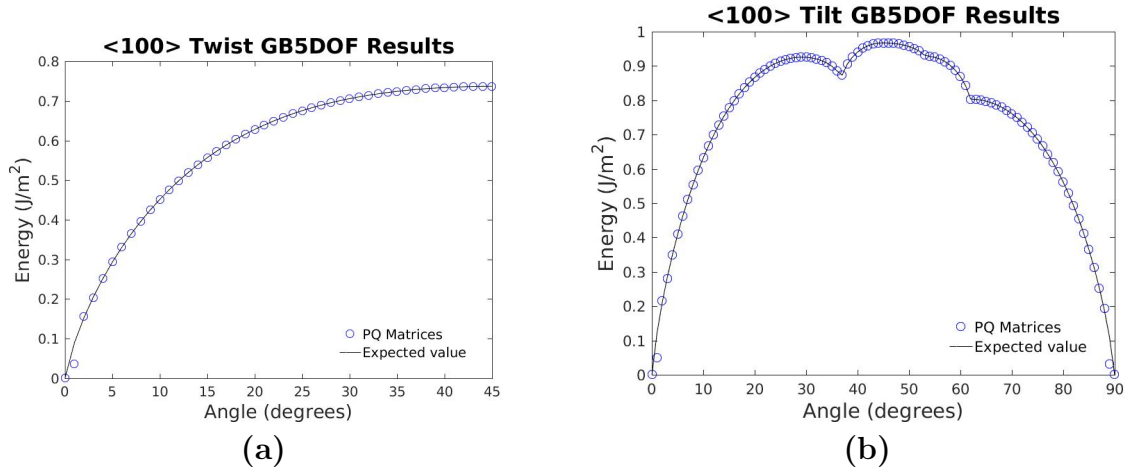


**Figure 3.1** The  $\langle 100 \rangle$  twist (a) and tilt (b) results for the P and Q matrices as compared to Bulatov *et al.*'s energy profiles. The expected value was calculated using Bulatov *et al.*'s GB5DOF.m MATLAB<sup>®</sup> script with the default values. The calculated values were found by inputting the matrices into the GB5DOF.m script. With the exception of the data points at  $1^\circ$  in both (a) and (b) and  $89^\circ$  in (b), the energies calculated from the matrices matches the expected curves exactly.

(Figure 3.2b) showed a deep cusp around  $28^\circ$  which was unexpected. An analysis of the molecular dynamics (MD) simulation results for this misorientation revealed, in this case, that the two crystals had realigned during the simulation due to abnormally high pressures. This realignment caused the misorientation angle to change causing the GB energy to be much lower than expected. Comparison with Harbison's simulation result revealed that the crystal structure from his simulation did not realign. While Harbison's data was not calculated with the anneal and thus may not represent a global minimum, the data point follows the surrounding data's trend, justifying the use of his result.

Of the symmetric tilt GB energy sets, the  $\langle 110 \rangle$  set has the most improvement. All three sets showed a general decrease in the energy, increasing confidence in the accuracy of the fit for GB energies in uranium dioxide ( $\text{UO}_2$ ). However, each of these sets provides more opportunity for research. The  $\langle 100 \rangle$  set needs more work done for data points after around  $50^\circ$ . The scatter associated with those points seems to be higher, and the possibility of a slight cusp presents itself around  $68^\circ$ . It is unknown what behaviors are expected there



though because there are so few data points in that region, so additional data would be beneficial. The  $\langle 110 \rangle$  set as mentioned shows the most improvement, but there are some low points in the second and third “humps” not following the trend, indicating further possibility for cusps. The first part of the function (the first hump) needs additional data to determine the possibility of a cusp between  $40^\circ$  and  $50^\circ$ . The fitted curve to the  $\langle 111 \rangle$  set now has an unexpected upward trend. The scatter associated with these data points is also relatively high, leading to the possibility of a completely different set of functions to define this subset.

The twist GB energy sets vary in their success. The  $\langle 100 \rangle$  set shows little difference between Harbison’s<sup>8</sup> work and this work. There is a slight positive concavity at the end of the fitting for this subset, which is unexpected, indicating the possibility of a cusp. This cusp may occur around  $30^\circ$ . The  $\langle 110 \rangle$  set has a definite decrease in the overall energies, creating a plateau profile. An additional cusp around  $40^\circ$  is being considered. The  $\langle 111 \rangle$  set has the least improvement. From the Bulatov *et al.*’s work<sup>1</sup> this work expected to see a plateau as Harbison’s fitting demonstrated.<sup>8</sup> Instead, the fitting produced a curved energy profile, indicating the potential for at least one cusp. A possible location of this cusp is around  $35^\circ$ . Preliminary work has been done with changing the number of parameters in an effort to maximize the quality of the fit with a minimal number of parameters. Figure 3.4 compares the current fitting to the tentative new fitting for three of the six 1D subsets. These modified fits in general seem to fit better at the cost of additional parameters, with a smaller  $\chi_{\text{red}}^2$  value. Still more parameters may be needed to accommodate additional cusps however.

Figure 3.3 shows the comparison between the values calculated from the P and Q matrices and the expected values from the MD calculations for the  $\langle 100 \rangle$  subset. All six subsets are shown in Figures B.7 to B.9 in Appendix B. There is an unsolved scaling issue with the  $\langle 100 \rangle$  tilt subset. Overall, the results from the P and Q matrices match the fitted values, with a few anomalies needing to be addressed.

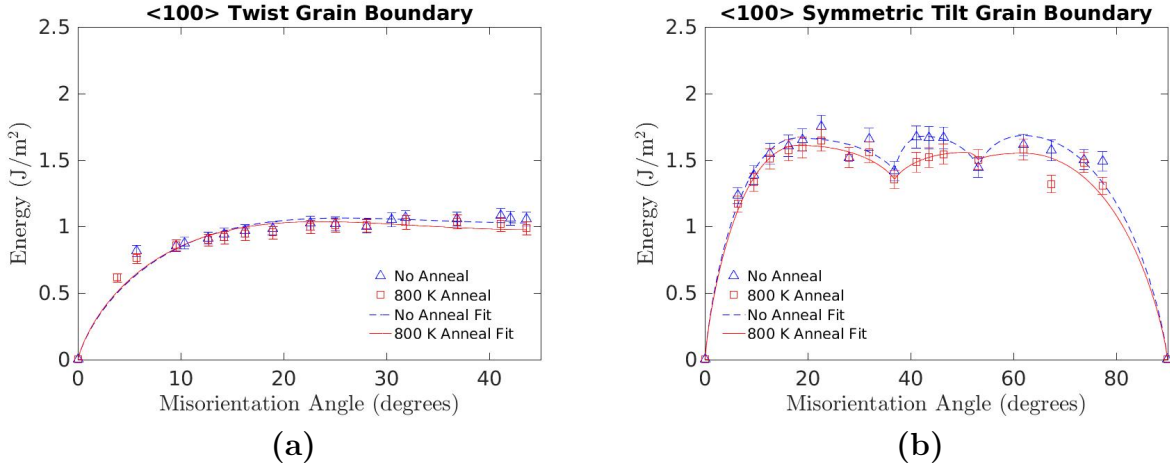


**Figure 3.2** The  $\langle 100 \rangle$  twist (a) and tilt (b) results. In general the re-calculated energies are lower, with significant differences around  $40^\circ$  to  $50^\circ$  in the tilt subset. The positive concavity in the twist subset around  $40^\circ$  is unexpected, and may indicate the presence of a missing cusp. There is a possible cusp around  $30^\circ$  in the twist subset, and around  $68^\circ$  in the tilt subset.

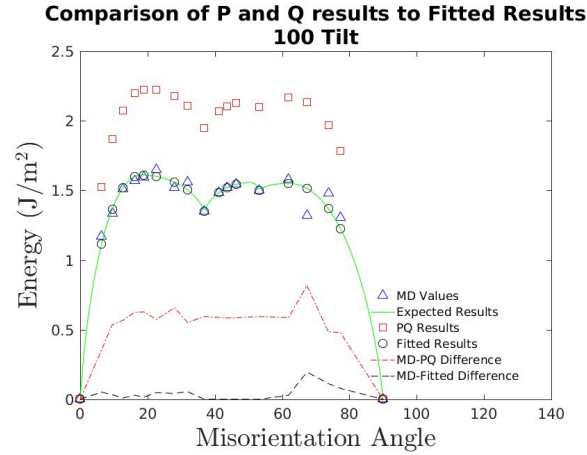


**Figure 3.3** A comparison of the expected value of the fitted function with the values calculated using the P and Q matrices for the  $\langle 100 \rangle$  1D tilt subset. The MD values are shown for reference. There is a scaling issue yet to be fixed, but it is uncertain what is causing the scaling issue for this subset.

### 3.3 Reduced Chi-square Results

The  $\chi_{\text{red}}^2$  values are much smaller than one for every data set regardless of the method used to calculate the statistic, with the exception of the  $\langle 100 \rangle$  symmetric tilt subset using the P and Q matrices. This subset has a high  $\chi_{\text{red}}^2$  value due to the scaling issue. Because of the

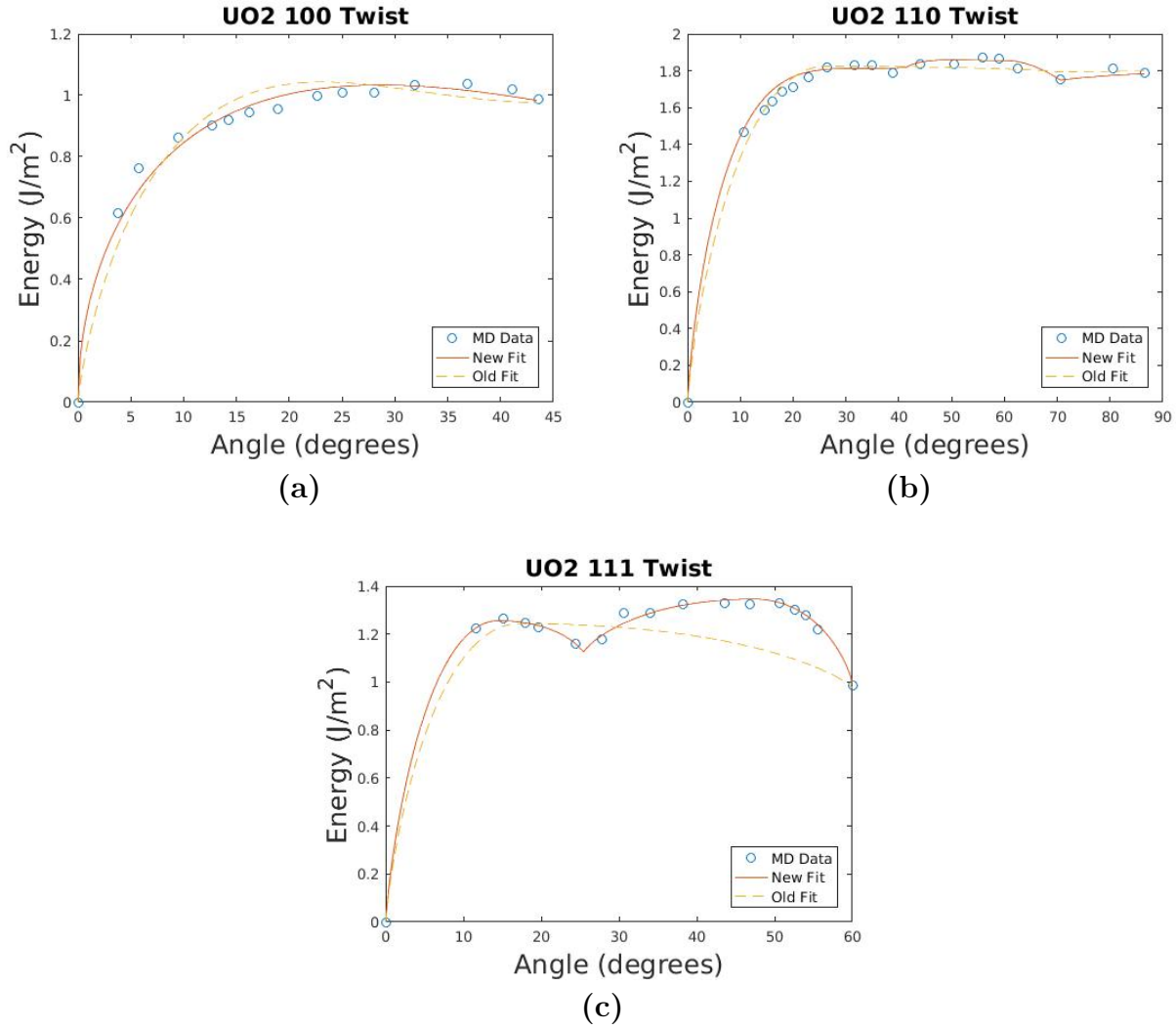


**Figure 3.4** An comparison of current fitting functions with a possible change to the functions. Original functions are shown as the dashed lines, with the updated functions shown as the solid lines. MD results are shown for reference. (a) shows a possible change from the Read-Shockley-Wolf (RSW) functions to a simple square root function multiplied by an exponential decay. There is no theoretical basis behind this change however. (b) attempts to fit to a cusp around 40°. Further work can be done to find a better fit for this subset. (c) shows the most potential improvement. The potential fit increases the total number of parameters by three to fit to the cusp around 28°. A quick glance at the MD values compared to the fit shows a great improvement from the current fit.

low  $\chi_{\text{red}}^2$  values, the fitted functions are known to overfit the data.<sup>23</sup> Table 3.1 lists the  $\chi_{\text{red}}^2$  values for the 1D subsets using the two different methods for calculation. Equation (3.1)

shows the equation used to calculate the  $\chi_{\text{red}}^2$  value:

$$\chi_{\text{red}}^2 = \frac{1}{N - n - 1} \sum \frac{(\epsilon_{\text{md}} - \epsilon)^2}{e \epsilon_{\text{md}}}. \quad (3.1)$$

In this equation,  $N$  is the number of observations,  $n$  is the number of parameters,  $\epsilon_{\text{md}}$  are the energies from MD,  $\epsilon$  are the energies from the model, and  $e$  is the uncertainty in the MD results.

**Table 3.1** A list of the  $\chi_{\text{red}}^2$  results using two different methods: using the P and Q matrices for the various orientations to test the fit, and comparing the results of the 1D fits to the 1D data. The values for  $\chi_{\text{red}}^2$  are all less than one with the exception of the  $\langle 100 \rangle$  symmetric tilt using the P and Q matrices. These values indicate an over-fit to the data.

1D Subset	$\chi_{\text{red}}^2$ using P and Q matrices		$\chi_{\text{red}}^2$ comparing the 1D fits	
	No Anneal	800 K Anneal	No Anneal	800 K Anneal
$\langle 100 \rangle$ Twist	0.0953	0.1074	0.0752	0.0722
$\langle 110 \rangle$ Twist	0.1010	0.1874	0.0400	0.0137
$\langle 111 \rangle$ Twist	0.3041	0.1139	0.4966	0.1516
$\langle 100 \rangle$ Tilt	0.1038	8.7702	0.0846	0.0932
$\langle 110 \rangle$ Tilt	4.9799	0.3277	0.5951	0.1762
$\langle 111 \rangle$ Tilt	0.1566	0.7814	0.1315	0.1355
Overall $\chi_{\text{red}}^2$	1.7652	1.4893	0.2678	0.1153

# Chapter 4

## Conclusion

This work has successfully created a more accurate interpolation function for grain boundary (GB) energies in uranium dioxide ( $\text{UO}_2$ ), but additional characteristics of the full five-dimensional (5D) GB space have been revealed that require further research. GB energies were found to be lower when calculated with an 800 K anneal as expected when compared to the data set created without an anneal, but additional characteristics of the GB energy space have become apparent and require further research. Descriptions of those additional characteristics through the use of additional functions will prove beneficial.

The most important work yet to be done is calculation of additional data points for fitting. Increasing the number of data points will improve the  $\chi^2_{\text{red}}$  value of the fit. Additional data points will also help to identify trends that do not readily appear with the limited data currently available. The difficulty associated with calculating additional data points is the required computational resources.

Further work could be done to generalize this function to all polycrystalline materials with the fluorite crystal structure. Such a generalization would provide further validation of this model, however, such validation would require a sufficient number of GB energies for many different materials with such a structure. As these energies are not already available in the literature, this would require additional computational resources. As the parameters

for GB energy interpolation are improved and validated, they should be incorporated into MARMOT to further the anisotropic grain growth model being developed.

# Bibliography

- <sup>1</sup> V. V. Bulatov, B. W. Reed and M. Kumar, *Grain boundary energy function for fcc metals*, Acta Mater. **65** (2014), pp. 161–175
- <sup>2</sup> V. Randle and O. Engler, *Introduction to Texture Analysis: Macrotexture, Microtexture and Orientation Mapping* (CRC Press, USA, 2000)
- <sup>3</sup> W. D. Callister Jr., *Materials Science and Engineering: An Introduction* (John Wiley & Sons Inc, USA, 2003)
- <sup>4</sup> Thomas Jefferson National Accelerator Facility – Office of Science Education, *The Element Uranium*, [education.jlab.org/itselemental/ele092.html](http://education.jlab.org/itselemental/ele092.html), Accessed: 13 October 2016
- <sup>5</sup> S. Patala and C. A. Schuh, *Symmetries in the representation of grain boundary-plane distributions*, Philosophical Magazine **93** (2013), pp. 524–573
- <sup>6</sup> P. Lejček, *Grain Boundaries: Description, Structure and Thermodynamics* (Springer Berlin Heidelberg, Berlin, Heidelberg, 2010), pp. 5–24
- <sup>7</sup> E. R. Homer, S. Patala and J. L. Priedeman, *Grain boundary plane orientation fundamental zones and structure-property relationships*, Sci. Rep. **5** (2015), p. 15476
- <sup>8</sup> T. Harbison, *Anisotropic grain boundary energy function for uranium dioxide*, B.S. Thesis, Brigham Young University - Idaho (2015)
- <sup>9</sup> G. S. Rohrer, *Grain Boundary Energy Anisotropy: A Review*, J. Mater. Sci. **46** (2011), pp. 5881–5895

- <sup>10</sup> Y. Zhang, *Unpublished*, Personal Communication
- <sup>11</sup> E. Hansen, *Unpublished*, Personal Communication
- <sup>12</sup> S. Plimpton, *Fast Parallel Algorithms for Short-Range Molecular Dynamics*, Journal of Computational Physics **117** (1995), pp. 1–19
- <sup>13</sup> A. S. Butterfield, *Exploration of the phase-field framework MARMOT to include anisotropic grain boundaries with molecular dynamics*, B.S. Thesis, Brigham Young University - Idaho (2013)
- <sup>14</sup> H. T. Stokes, *Solid State Physics: For advanced undergraduate students* (BYU Academic Publishing, Provo, Utah, 2007)
- <sup>15</sup> W. T. Read and W. Shockley, *Dislocation models of crystal grain boundaries*, Physical Review **78** (1950), pp. 275–289
- <sup>16</sup> D. Wolf, *A Read–Shockley model for high–angle grain boundaries*, Scripta Metallurgica **23** (1989), pp. 1713–1718
- <sup>17</sup> F. C. Frank, *Orientation Mapping*, Metallurgical Transactions A **19A** (1988), pp. 403–408
- <sup>18</sup> A. Morawiec and D. P. Field, *Rodrigues parameterization for orientation and misorientation distributions*, Phil. Mag. A **73** (1996), pp. 1113–1130
- <sup>19</sup> R. Becker and S. Panchanadeeswaran, *Crystal rotations represented as Rodrigues vectors*, Textures and Microstructures **10** (1989), pp. 167–194
- <sup>20</sup> L. Priester, *Geometrical Order of Grain Boundaries* (Springer Netherlands, Dordrecht, 2013), pp. 3–28
- <sup>21</sup> D. M. Kirch, *Fundamentals of grain boundaries and triple junctions* (Cuvillier, Göttingen, 2008), pp. 1–7



- <sup>22</sup> S. Patala, J. K. Mason and C. A. Schuh, *Improved representations of misorientation information for grain boundary science and engineering*, Progress in Materials Science **57** (2012), pp. 1383–1425
- <sup>23</sup> P. R. Bevington and D. K. Robison, *Data Reduction and Error Analysis for the Physical Sciences* (McGraw–Hill, New York, NY, 2003)
- <sup>24</sup> M. R. Tonks, D. Gaston, P. C. Millett, D. Andrs and P. Talbot, *An object-oriented finite element framework for multiphysics phase field simulations*, Computational Materials Science **51** (2012), pp. 20–29
- <sup>25</sup> S. Belongie, *Rodrigues Rotation Formula From MathWorld—A Wolfram Web Resource*, created by Eric W. Weisstein (2006), [mathworld.wolfram.com/RodriguesRotationFormula.html](http://mathworld.wolfram.com/RodriguesRotationFormula.html)
- <sup>26</sup> F. Bachmann, R. Hielscher and H. Schaeben, *Texture Analysis with MTEX – Free and Open Source Software Toolbox*, Solid State Phenomena **160** (2010), pp. 63–68
- <sup>27</sup> E. W. Weisstein, *Quaternion From MathWorld—A Wolfram Web Resource* (2004), [mathworld.wolfram.com/Quaternion.html](http://mathworld.wolfram.com/Quaternion.html)



# Appendix A

## List of Parameters

**Table A.1** This table gives the parameters for  $\text{UO}_2$  generating the energy function.

Array number	Parameter name	Parameter value
1	Energy Scaling Factor ( $e_{RGB}$ )	$1.6012 \text{ J/m}^2$
2	$\langle 100 \rangle$ Max Distance	0.405
3	$\langle 110 \rangle$ Max Distance	0.739
4	$\langle 111 \rangle$ Max Distance	0.352
5	$\langle 100 \rangle$ Weight	50.5
6	$\langle 110 \rangle$ Weight	4.55
7	$\langle 111 \rangle$ Weight	0.08
8	$\langle 100 \rangle$ Tilt/Twist Mix Power Law (1)	0.03325
9	$\langle 100 \rangle$ Tilt/Twist Mix Power Law (2)	0.00053125
10	Maximum $\langle 100 \rangle$ Twist Energy	0.60903
11	$\langle 100 \rangle$ Twist Shape Factor	1.4486
12	$\langle 100 \rangle$ Asymmetric Tilt Interpolation Power	35.8
13	$\langle 100 \rangle$ Symmetric Tilt First Peak Energy	1.0058

*Continued on next page.*

Table A.1 – *Continued from previous page*

Array number	Parameter name	Parameter value
14	$\langle 100 \rangle$ Symmetric Tilt First $\Sigma 5$ Energy	0.84456
15	$\langle 100 \rangle$ Symmetric Tilt Second Peak Energy	0.97259
16	$\langle 100 \rangle$ Symmetric Tilt Second $\Sigma 5$ Energy	0.9379
17	$\langle 100 \rangle$ Symmetric Tilt $\Sigma 17$ Energy	0.96881
18	$\langle 100 \rangle$ Symmetric Tilt First Peak Angle	0.31569
19	$\langle 100 \rangle$ Symmetric Tilt Second Peak Angle	0.88538
20	$\langle 110 \rangle$ Tilt/Twist Mix Power Law (1)	3.1573
21	$\langle 110 \rangle$ Tilt/Twist Mix Power Law (2)	1.9784
22	$\langle 110 \rangle$ Twist Peak Angle	0.46145
23	$\langle 110 \rangle$ Twist Peak Energy	1.1444
24	$\langle 110 \rangle$ Twist $\Sigma 3$ Energy	1.0931
25	$\langle 110 \rangle$ Twist $90^\circ$ Energy	1.152
26	$\langle 110 \rangle$ Asymmetric Tilt Shape Factor	3.1843
27	$\langle 110 \rangle$ Symmetric Tilt Third Peak Energy	1.0514
28	$\langle 110 \rangle$ Symmetric Tilt $\Sigma 3$ Energy	0.61703
29	$\langle 110 \rangle$ Symmetric Tilt Second Peak Energy	1.0902
30	$\langle 110 \rangle$ Symmetric Tilt $\Sigma 11$ Energy	0.56686
31	$\langle 110 \rangle$ Symmetric Tilt First Peak Energy	1.1024
32	$\langle 110 \rangle$ Symmetric Tilt Third Peak Angle	0.88736
33	$\langle 110 \rangle$ Symmetric Tilt Second Peak Angle	1.8711
34	$\langle 110 \rangle$ Symmetric Tilt First Peak Angle	2.731
35	$\langle 111 \rangle$ Tilt-Twist Linear Interpolation	38.201
36	$\langle 111 \rangle$ Twist Shape Factor	1.2414
37	$\langle 111 \rangle$ Twist Peak Angle	0.49979

*Continued on next page.*

Table A.1 – *Continued from previous page*

Array number	Parameter name	Parameter value
38	$\langle 111 \rangle$ Twist Peak Energy	0.7971
39	$\langle 111 \rangle$ Symmetric Tilt Peak Angle	0.25966
40	$\langle 111 \rangle$ Symmetric Tilt Max Energy	1.0288
41	$\langle 111 \rangle$ Symmetric Tilt $\Sigma 3$ Energy	1.1311
42	$\langle 111 \rangle$ Asymmetric Tilt Symmetry Point Energy	3.7674
43	$\langle 111 \rangle$ Asymmetric Tilt Scale Factor	0.053417



# Appendix B

## Graphs

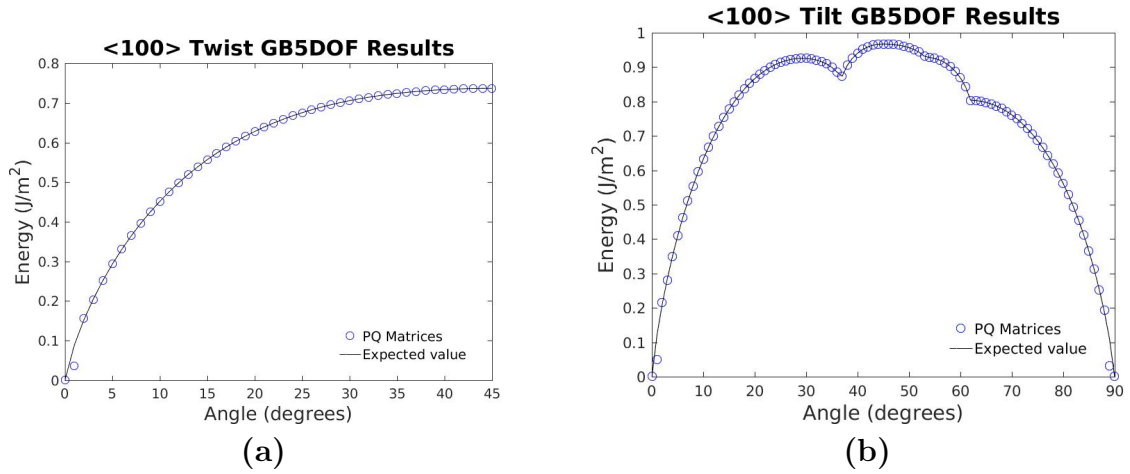


**Figure B.1** The  $\langle 100 \rangle$  twist (a) and tilt (b) results for the P and Q matrices as compared to Bulatov *et al.*'s energy profiles. The expected value was calculated using Bulatov *et al.*'s GB5DOF.m MATLAB<sup>®</sup> script with the default values. The calculated values were found by inputting the matrices into the GB5DOF.m script. With the exception of the data points at  $1^\circ$  in both (a) and (b) and  $89^\circ$  in (b), the energies calculated from the matrices matches the expected curves exactly.

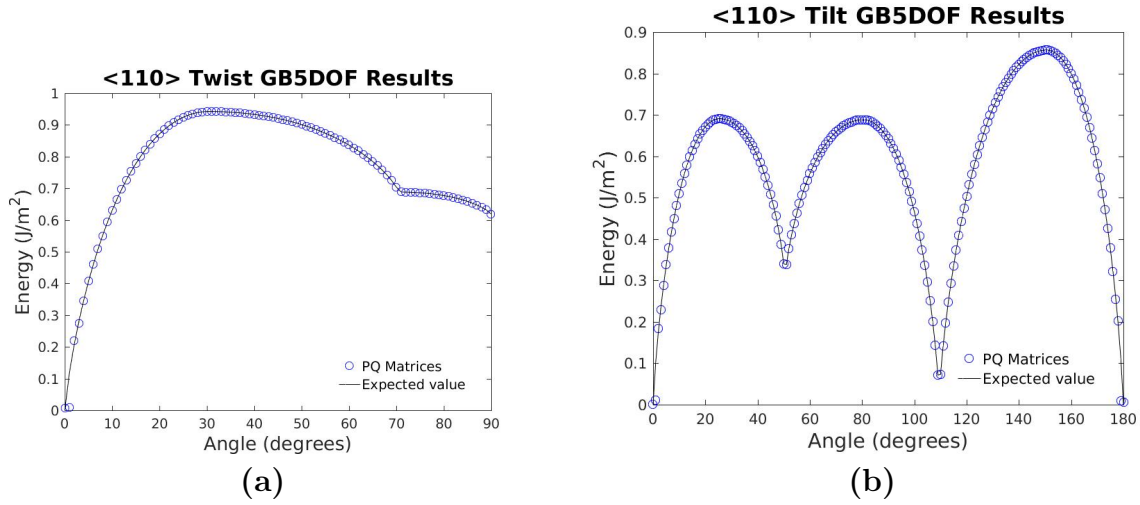


**Figure B.2** The  $\langle 110 \rangle$  twist (a) and tilt (b) results for the P and Q matrices as compared to Bulatov *et al.*'s energy profiles. The expected value was calculated using Bulatov *et al.*'s GB5DOF.m MATLAB<sup>®</sup> script with the default values. The calculated values were found by inputting the matrices into the GB5DOF.m script. With the exception of the data points at  $1^\circ$  in both (a) and (b) and  $179^\circ$  in (b), the energies calculated from the matrices matches the expected curves exactly.

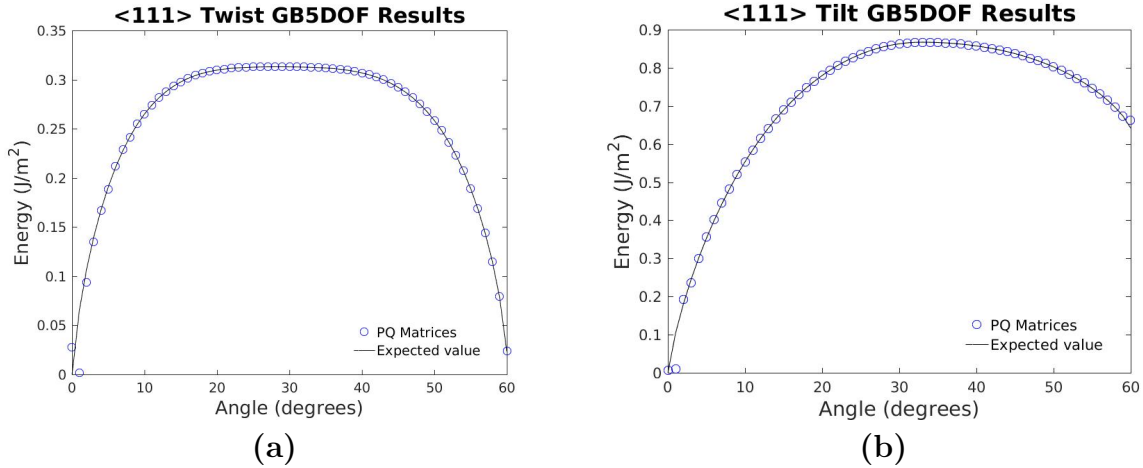


**Figure B.3** The  $\langle 111 \rangle$  twist (a) and tilt (b) results for the P and Q matrices as compared to Bulatov *et al.*'s energy profiles. The expected value was calculated using Bulatov *et al.*'s GB5DOF.m MATLAB<sup>®</sup> script with the default values. The calculated values were found by inputting the matrices into the GB5DOF.m script. With the exception of the data points at  $1^\circ$  in both (a) and (b) and  $60^\circ$  in (b), the energies calculated from the matrices matches the expected curves exactly.



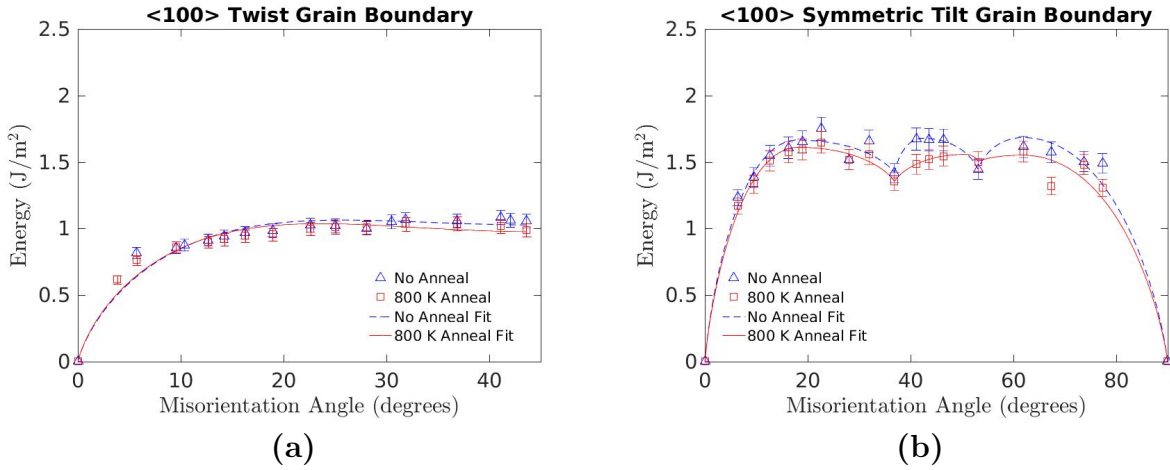


**Figure B.4** The  $\langle 100 \rangle$  twist (a) and tilt (b) results. In general the re-calculated energies are lower, with significant differences around  $40^\circ$  to  $50^\circ$  in the tilt subset. The positive concavity in the twist subset around  $40^\circ$  is unexpected, and may indicate the presence of a missing cusp. There is a possible cusp around  $30^\circ$  in the twist subset, and around  $68^\circ$  in the tilt subset.

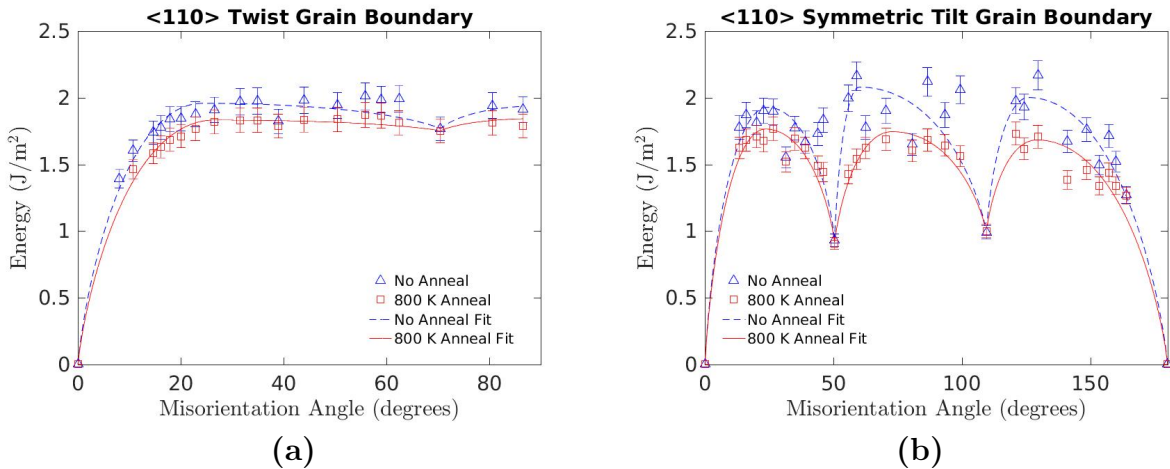


**Figure B.5** The  $\langle 110 \rangle$  twist (a) and tilt (b) results. Significant decreases in energy are found for both subsets. Possible cusp locations are around  $40^\circ$  in the twist subset, and around  $40^\circ$ ,  $90^\circ$ , and  $140^\circ$  in the tilt subset.

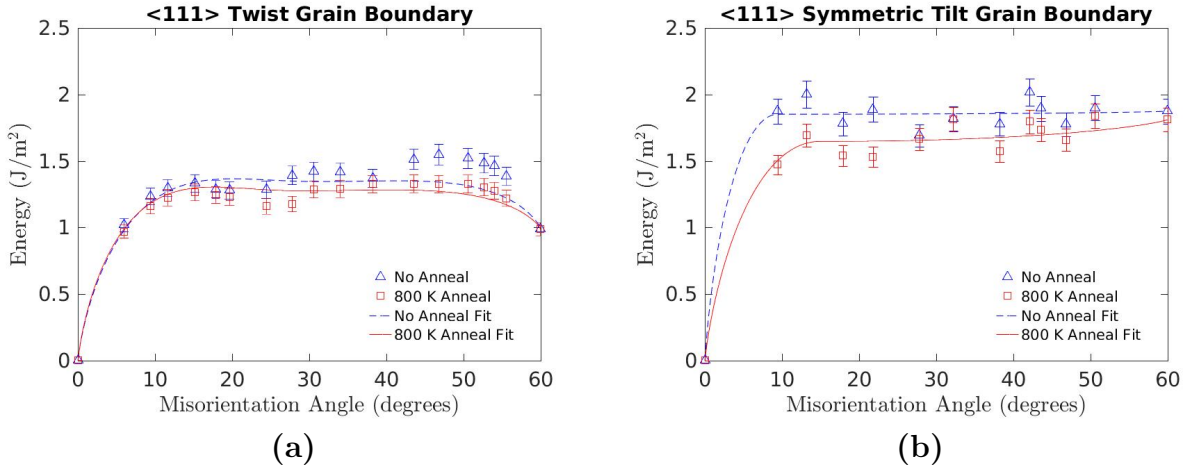


**Figure B.6** The  $\langle 111 \rangle$  twist (a) and tilt (b) results. Some energies are found to be lower, but some are also found to be higher. The positive concavity present in these results is unexpected, and could indicate the presence of cusps. A possible location for the twist subset is around  $33^\circ$ . Additional data is needed to determine possible cusp locations for the tilt subset.

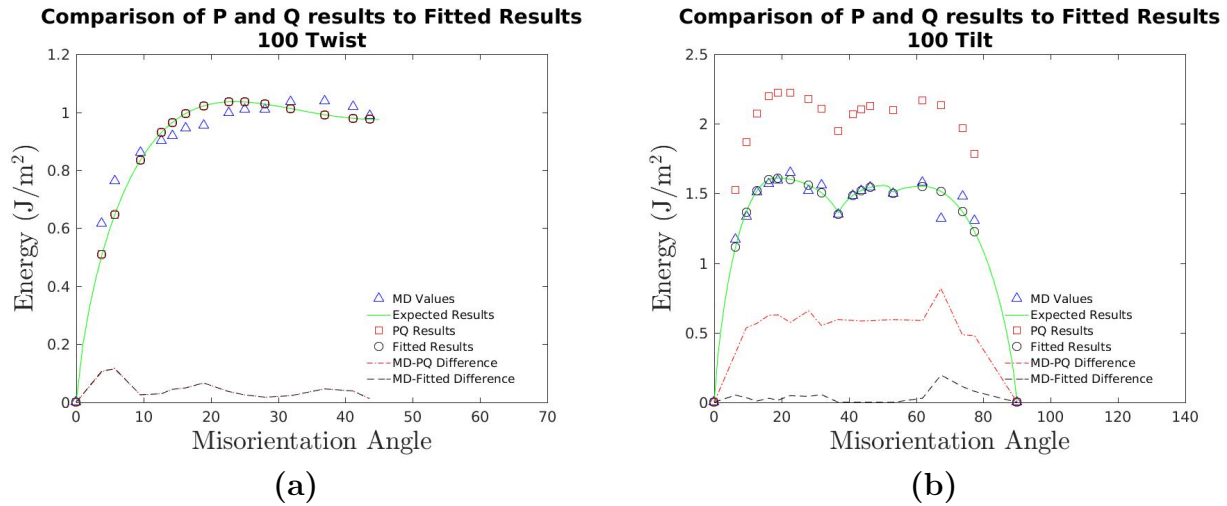


**Figure B.7** A comparison of the expected value of the fitted function with the values calculated using the P and Q matrices for the  $\langle 100 \rangle$  1D subsets. The MD values are shown for reference. (a) PQ results follow exactly the fitted curve. (b) has a scaling issue yet to be fixed. It is uncertain what is causing the scaling issue for this subset.

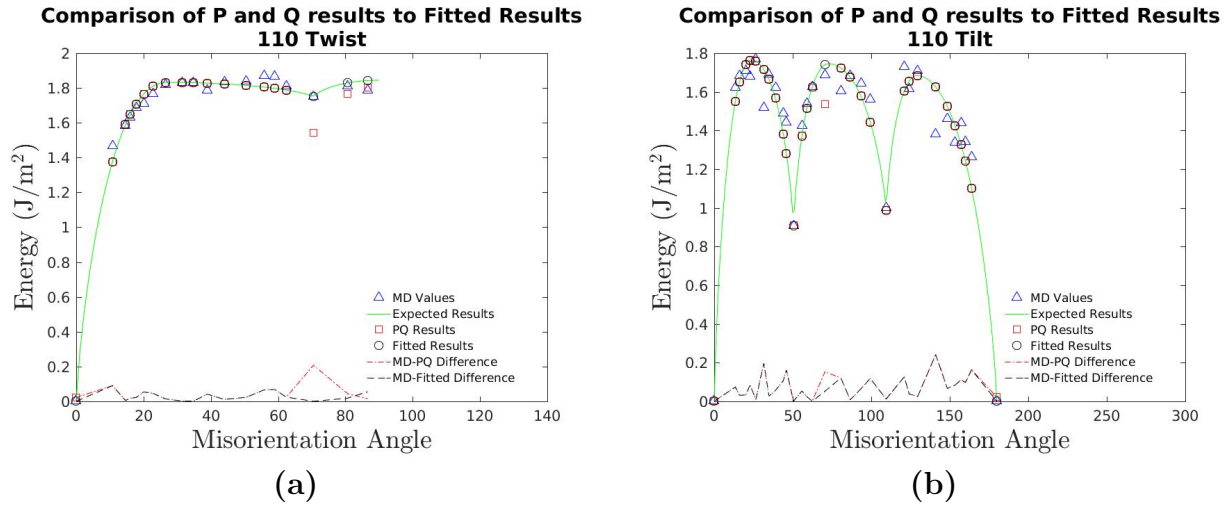


**Figure B.8** A comparison of the expected value of the fitted function with the values calculated using the P and Q matrices for the  $\langle 110 \rangle$  1D subsets. MD values are shown for reference. (a) follows the fitted result until the cusp, at which point some anomalies appear. The results from the PQ matrices dip well below the expected value at the cusp, and never make it back to the original fitted line. (b) has a similar issue on a lesser scale. Only two of the calculated points do not follow the fitted curve. The endpoint is expected to return a zero value, where the PQ matrices calculated a value slightly higher. There is also an unexpected cusp from the PQ matrices in the middle of the second hump. All other data points follow the fitted curve exactly.

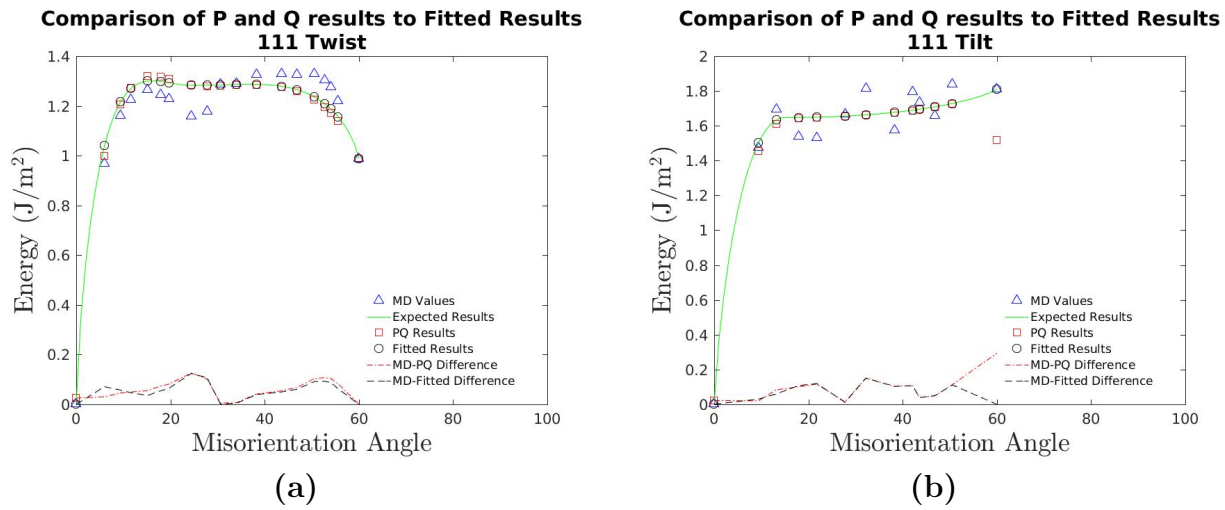


**Figure B.9** A comparison of the expected value of the fitted function with the values calculated using the P and Q matrices for the  $\langle 111 \rangle$  1D subsets. MD values are shown for reference. (a) closely follows the expected fitted values, but has a slight error throughout. (b) follows the expected values exactly in the center of the fitting, but misses slightly for lower angle boundaries, and misses completely at the end.

# Appendix C

## Orientation Matrix Generator

This code generates the orientation matrices (known as the P and Q matrices in Bulatov *et al.*'s code). Provision for calculating the matrices one of two ways is provided in-code through the use of command-line options.

```
#!/usr/bin/env python

# This script will calculate the orientation matrices for any
#   given misorientation
# for any of the high-symmetry axes.
# Arguments:
#
#   _axis: The axis of orientation (type: int)
#   _misorientation: The angle of misorientation (type: float)
#
#           —————OR—————
#   (with option -e or --euler)
#   _z1: The first rotation angle (Z ) (type: float)
#   _x:  The second rotation angle (X') (type: float)
#   _z2: The third rotation angle (Z'') (type: float)
```

```

#
# If the option -e or --euler-angles is entered, the calculation
# skips to simply
# output the orientation matrices. Otherwise, the Euler angles
# are calculated from
# the axis, orientation, and grain boundary normal, and then the
# orientation matrix is
# created through the use of the Rodrigues Rotation Formula, which
# is:
#  $R = I + \sin(\theta) * K + (1 - \cos(\theta)) * K^2$ 
# where  $I$  is the identity matrix,  $\theta$  is the misorientation
# angle, and  $K$  is
# the skew-symmetric matrix formed by the axis of rotation:
#  $K = \begin{pmatrix} 0 & -k_z & k_y \\ k_z & 0 & -k_x \\ -k_y & k_x & 0 \end{pmatrix}$ 
# where the vector  $k$  is the unit vector defining the axis of
# rotation, or using
# a set of predefined rotations for each axis (default is the
# predefined rotations).
# The Euler angles are calculated in this case simply for the file
# to be written
# to. If the user does not specify to save, then the angles are
# not used for
# anything.
#
# Options:

```

---

```

# -e —euler <_z1> <_x> <_z2>           Returns the Bunge
orientation matrix
#                                           based on the euler angles
provided.
#
# -f —file <filename>                   Reads the file filename
and uses the
#                                           Euler angles from them to
calculate the
#                                           orientation matrix.
#
# —rrf                                   Calculates the matrices
using the Rodrigues
#                                           Rotation Formula
#
# -a —angles                             Displays the Euler angles.
Can be used
#                                           in conjunction with -q or
—quiet to
#                                           display only the Euler
angles.
#
# -s —save                               Saves the resultant
orientation matrix to
#                                           a database (
orientation_matrix_database.m)

```

```

#                                     with the accompanying
    Euler angles.

#

# -q —quiet                         Suppresses output of the
    orientation matrices

#                                     to the terminal

#

# —help                             Displays this help info

#

# Output:

# For an Euler angle set, the output is simply its orientation
    matrix.

# For the misorientations, the first matrix is the 'P' orientation
    matrix, and

# the second matrix is the 'Q' orientation matrix (see Bulatov et
    al., Acta Mater
    # 65 (2014) 161–175).

from __future__ import division, print_function # To avoid
    numerical problems with division, and for ease of printing

from sys import argv # for CLI arguments

from math import cos, sin, pi, atan2, sqrt # Trig functions

from os.path import exists # For checking existence of a file

from numpy import array, linalg

from myModules import * # imports my functions from the file
    myModules.py

```



---

*# Helper functions*

**def** displayHelp():

**print**( '''

*This script will calculate the orientation matrices for any  
given misorientation*

*for any of the high-symmetry axes.*

*Arguments:*

*\_axis: The axis of orientation (type: int)*

*\_misorientation: The angle of misorientation (type: float)*

*—————OR—————*

*(with option -e or —euler)*

*\_z1: The first rotation angle (Z ) (type: float)*

*\_x: The second rotation angle (X') (type: float)*

*\_z2: The third rotation angle (Z'') (type: float)*

*If the option -e or —euler-angles is entered, the calculation  
skips to simply*

*output the orientation matrices. Otherwise, the Euler angles  
are calculated from*

*the axis, orientation, and grain boundary normal, and then the  
orientation matrix is*

*created through the use of the Rodrigues Rotation Formula,  
which is:*

$$R = I + \sin(\theta) * K + (1 - \cos(\theta)) * K^2$$

*where I is the identity matrix, theta is the misorientation  
angle, and K is*

*the skew-symmetric matrix formed by the axis of rotation:*

$$K = \begin{pmatrix} 0 & -kz & ky \\ kz & 0 & -kx \\ -ky & kx & 0 \end{pmatrix}$$

*where the vector  $k$  is the unit vector defining the axis of rotation, or using*

*a set of predefined rotations for each axis (default is the predefined rotations).*

*The Euler angles are calculated in this case simply for the file to be written*

*to. If the user does not specify to save, then the angles are not used for anything.*

*Options:*

*-e —euler <\_z1> <\_x> <\_z2>  
orientation matrix*

*Returns the Bunge*

*based on the euler angles  
provided.*

*-f —file <filename>  
and uses the*

*Reads the file filename*

*Euler angles from them to  
calculate the  
orientation matrix.*

*—rrf*  
*using the Rodrigues*

*Calculates the matrices*

*Rotation Formula*

*—a —angles*  
*Can be used*

*Displays the Euler angles.*

*in conjunction with —q or*  
*—quiet to*  
*display only the Euler*  
*angles.*

*—s —save*  
*orientation matrix to*

*Saves the resultant*

*a database (*  
*orientation\_matrix\_database*  
*.m)*  
*with the accompanying*  
*Euler angles.*

*—q —quiet*  
*orientation matrices*

*Suppresses output of the*  
*to the terminal*

*—help*

*Displays this help info*

*Output:*

*For an Euler angle set, the output is simply its orientation matrix.*

*For the misorientations, the first matrix is the 'P' orientation matrix, and the second matrix is the 'Q' orientation matrix (see Bulatov et al., Acta Mater 65 (2014) 161–175).*

```
'''
return

def displayAngles(z1, x, z2): # Displays an Euler angle set (Bunge
    convention)
    print("Euler_angles:")
    # This is the "new" way to format strings. The 16 indicates
        the padding to
    # be done before the next character. The '<' character below
        says which side
    # to pad (the right side).
    print("{:16}{:16}{:16}".format('Z', 'X', 'Z'))
    print("_____")
    print("{:<16}{:<16}{:<16}\n".format(rad2deg(z1), rad2deg(x),
        rad2deg(z2)))
    return

def check4RRF(args): # Check the args for the rrf command
    if "--rrf" in args:
        index = args.index("--rrf")
```

```
        del args[index]

        return True, args

    else:

        return False, args


def check4Euler(args): # Check the args for the -a or --angles
command

    if "-a" in args or "--angles" in args:

        try:

            index = args.index("-a")

        except:

            index = args.index("--angles")

        del args[index]

        return True, args

    else:

        return False, args


# Write the matrix and angles to a file

def writeMat(m, _z1, _x, _z2, grain, axis):

    # This is to avoid issues with duplicates

    if _z1 == 0:

        _z1 = abs(_z1)

    if _x == 0:

        _x = abs(_x)

    if _z2 == 0:

        _z2 = abs(_z2)
```

```

lastVal = 1

# This is the default filename to be used.

# TODO: make provisions to provide the database file via
      command line

tex_filename = "orientation_matrix_database.m"

var_name = "%s%d"%(grain, axis) # Will generally look like
      P100 or Q100

if not exists(tex_filename):

    tex_file = open(tex_filename, "a")

    tex_file.write("%Database_for_orientation_matrices_for_
        specified_Euler_Angles\n")

    tex_file.write("
        %
        _____
        n")

    tex_file.write("%Orientation_Matrix_
        _____
        _____Euler_Angles\n")

    tex_file.write("%s(:, :, %d)=[%2.6f__%2.6f__%2.6f__
        _____
        %%%2.4f__%2.4f__%2.4f\n"%(var_name, lastVal, m[0][0], m
        [0][1], m[0][2], _z1, _x, _z2))

    tex_file.write("%2.6f__%2.6f__%2.6f\n"%(m[1][0], m[1][1],
        m[1][2]))

    tex_file.write("%2.6f__%2.6f__%2.6f];\n"%(m[2][0], m
        [2][1], m[2][2]))

    tex_file.write("
        %
        _____
        n")

    tex_file.close()

```

---

```

else:
    f = open(tex_filename, "r")
    while True:
        data = f.readline().split()
        if not data:
            break
        elif len(data) != 6:
            continue
        else:
            assert data[0][0] in {'P', 'Q'}, "Unknown
            orientation_matrix_type (should be \ 'P\ ' or \ 'Q
            \')."
            if not "%d"%(axis) in data[0][1:4]:
                lastVal = 0
            elif "%d"%(axis) in data[0][1:4]:
                try:
                    try:
                        if data[0][0] == 'P': # Handles
                            anything 3 digits long
                            lastVal = int(data[0][9:12]) - 1
                    else:
                        lastVal = int(data[0][9:12])
                except:
                    if data[0][0] == 'P': # Handles
                        anything 2 digits long
                        lastVal = int(data[0][9:11]) - 1
                    else: # data[0][0] == 'Q'

```

```

        lastVal = int(data[0][9:11])

    except:

        if data[0][0] == 'P': # One digit case
            lastVal = int(data[0][9]) - 1
        else: # data[0][0] == 'Q'
            lastVal = int(data[0][9])

    else:

        print("Error: _Unknown_last_index.")
        exit()

# Checks to see if the Euler angles have already
# been used before

# If so, the calculated matrix is not saved (
# assumed to already
# be in the database)

if data[0][0] == grain and data[3] == ('%' + "%2.4
f"%_z1) and data[4] == "%2.4f"%_x and data[5]
== "%2.4f"%_z2:

    unique = False

    break

else:

    unique = True

if unique:

    tex_file = open(tex_filename, "a")

    tex_file.write("%s(:, :, %d)=[%2.6f__%2.6f__%2.6f____
____%2.4f__%2.4f__%2.4f\n"%(var_name, lastVal +
1, m[0][0], m[0][1], m[0][2], _z1, _x, _z2))

```



---

```

tex_file.write("%2.6f_ _%2.6f_ _%2.6f\n"%(m[1][0], m
            [1][1], m[1][2]))
tex_file.write("%2.6f_ _%2.6f_ _%2.6f];\n"%(m[2][0], m
            [2][1], m[2][2]))
tex_file.write("
%
n")
tex_file.close()

return

if "--help" in argv: # Help info
    displayHelp()
    exit()

orientation_matrix = []
save, argv = check4Save(argv) # Save the file? Delete the save
    argument
quiet, argv = check4Quiet(argv) # Checks for suppressing output.
    Delete the quiet argument.
useRRF, argv = check4RRF(argv) # Checks for using the RRF method.
    Delete the rrf argument.
dispEuler, argv = check4Euler(argv) # Checks for displaying the
    Euler angles. Delete the angle argument

# If the arguments come from a file ...
if "-f" in argv or "--file" in argv: #input arguments come from
    file

```

```

try:
    try:
        index = argv.index("-f")
    except:
        index = argv.index("--file")
except:
    print("ERROR: Unable to find filename.")
    exit()
filename = argv[index + 1]
try:
    fl = open(filename, 'r')
except:
    print("ERROR: Unable to read file.", filename)

while True: # Read the file line by line.
    line = fl.readline()
    # break if we don't read anything. If there are blank
    # lines in the
    # file, this will evaluate to TRUE!
    if not line:
        break;
    data = line.split()
    if len(data) != 4: # If there are less than 4 parts to the
        data, move along (format of file MUST be _z1 _x _z2
        1.00)
        continue
    else:

```

---

```

    # Convert the data to stuff we can use

    _z1 = float(data[0])
    _x  = float(data[1])
    _z2 = float(data[2])

    _z1 = deg2rad(_z1)
    _x  = deg2rad(_x)
    _z2 = deg2rad(_z2)
    orientation_matrix = calcRotMat(_z1, _x, _z2)

    if not quiet:
        displayMat(orientation_matrix)

    if save:
        writeMat(orientation_matrix, _z1, _x, _z2, 'P',
                 _axis)

# Input is a set of euler angles
elif "-e" in argv or "--euler-angles" in argv:
    try:
        try:
            index = argv.index("-e")
        except:
            index = argv.index("--euler-angles")
    except:
        print("ERROR: Unable to read Euler angles.")
        exit()

    _z1 = float(argv[index + 1])
    _x  = float(argv[index + 2])

```

```

_z2 = float(argv[index + 3])
_z1 = deg2rad(_z1)
_x  = deg2rad(_x)
_z2 = deg2rad(_z2)

orientation_matrix = calcRotMat(_z1, _x, _z2)

if not quiet:
    displayMat(orientation_matrix)
if save:
    writeMat(orientation_matrix, _z1, _x, _z2, 'P', _axis)

else:
    if len(argv) < 3:
        print("ERROR: _Not_enough_command_line_arguments.")
        print("Input _either _an _axis, _and _a _misorientation, _or _a _
            ZXZ Euler _angle _set _with _the _option _-e _or _--euler -
            angles.")
        displayHelp()
        exit()
    try:
        _axis = int(argv[1])
        _misorientation = float(argv[2])
    except:
        print( '''
        ERROR: Command line argument(s) is (are) not of correct
            type.

```

---

*Please enter an int for argument 1, a float for argument 2, and an int for argument 3.*

''')

exit()

```
if not len(str(_axis)) == 3: # axis length greater than 3
    print("ERROR: _Argument_1_must_by_a_3_digit_number_like_
          \ '100\ ' .")
    exit()
```

```
_misorientation = deg2rad(_misorientation) # Change input to
radians
```

```
axis = [None]*3
```

```
_z1 = [None]*2
```

```
_x = [None]*2
```

```
_z2 = [None]*2
```

```
q = [None]*2
```

```
for i in range(0, len(str(_axis))):
```

```
    axis[i] = int(str(_axis)[i])
```

```
#
```

---

```
#-----The Actual Calculations
```

```
-----#
```

```
#
```

---

```

# First convert to a quaternion
# These functions are from a myModules.py.
q[0] = axis2quat(axis, _misorientation / 2)
q[1] = axis2quat(axis, -_misorientation / 2)

# Convert the quaternion to Euler Angles
for i in range(0, len(_z1)):
    _z1[i], _x[i], _z2[i] = quat2euler(q[i])

#

```

---

```

# Using the Rodrigues Rotation Formula, defined as  $R = I + \sin(\theta) * K + (1 - \cos(\theta)) * K^2$ 
# with  $K = [0 \ -k_z \ k_y; k_z \ 0 \ -k_x; -k_y \ k_x \ 0]$ , and the
# components of
#  $k$  coming from the vector being rotated about.  $\theta$  is
# specified by the misorientation.
if useRRF:
    orientation_matrix1, orientation_matrix2 = calcRotMatRRF(
        axis, _misorientation)

    if not quiet:
        displayMat(orientation_matrix1)
        displayMat(orientation_matrix2)

```

---

```

    for i in range(0, len(_z1)):
        if dispEuler:
            displayAngles(_z1[i], _x[i], _z2[i])

        if save:
            assert i < 2, "ERROR: Too many Euler angles."
            if i == 0:
                writeMat(orientation_matrix1, _z1[i], _x[i],
                        _z2[i], 'P', _axis)
            else:
                writeMat(orientation_matrix2, _z1[i], _x[i],
                        _z2[i], 'Q', _axis)

#

```

---

```

else:
    for i in range(0, len(_z1)):
        orientation_matrix = calcRotMat(_z1[i], _x[i], _z2[i])

        if not quiet: # Display the results
            displayMat(orientation_matrix)

        if dispEuler: # Display the Euler Angles
            displayAngles(_z1[i], _x[i], _z2[i])

        if save: # We only calculate 2 angles at a time. If
            there are more, that's a problem.

```

```
assert i < 2, "ERROR: Too many Euler angles."
if i == 0:
    writeMat(orientation_matrix, _z1[i], _x[i],
             _z2[i], 'P', _axis)
else:
    writeMat(orientation_matrix, _z1[i], _x[i],
             _z2[i], 'Q', _axis)
```



# Appendix D

## genOrientationMatrix.sh Bash Script

This bash script reads a CSV file containing misorientation angles data, and uses those angles to generate the P and Q matrices. This script calls the script `orientation_matrix.py`.

```
#!/bin/bash

# This script will generate the orientation matrices through
# python by looping
# through the CSV values given in the input files.
# Argument(s):
#     $1          Should be a filename that specifies the angles and
#                  relative
#                  energies for the 100, 110, and 111 symmetric tilt
#                  and twist
#                  boundaries

# Command-line argument counter that checks for the correct number
# of arguments.
# Does not check for correct syntax.
```

```

if [ "$#" -ne 1 ]; then
    echo "Illegal number of parameters"
    exit 1
fi

# This takes the first argument from the command line - this is
# assumed to be a
# filename of the format 100Tilt.
FN=$1

echo "Determining the axis ..."
# Pulls out the axis from the input file name. This uses regex
# syntax to find
# a series of numbers that match either 100, 110, or 111. This
# also has an issue
# where it will find a match for 101, but as long as the files are
# named correctly
# it shouldn't be an issue.
AXIS=$(echo $FN | grep -o "1[01][01]" '

echo "Reading the file ..."
IFS="," # separation character is the comma
# Exit with error code 99 if unable to read the file
[ ! -f $FN ] && { echo "$FN file not found"; exit 99; }

# This makes the assumption that the file orientation_matrix.py
# has executable

```

```
# rights .  
  
echo "Running the command: ~/projects/scripts/orientation_matrix.  
    py $AXIS <angle> -s -q"  
  
while read -r angle en; do # read the file with comma separated  
    values  
  
    ~/projects/scripts/orientation_matrix.py $AXIS $angle -s -q  
  
done < "$FN" # the "$FN" is required if it's going to run properly  
!  
  
IFS=$OLDIFS # go back to the old separation character based on the  
    system value.
```

